

Mineralogical and Geochemical
Investigation of Silver and Cobalt
Trace Metals in the Mount Isa Copper
Deposit



Thesis submitted in accordance with the requirements of the University of
Adelaide for an Honours Degree in Geology

Cassandra Louise Lintvelt
October 2017

MINERALOGICAL INVESTIGATION OF SILVER AND COBALT TRACE METALS IN THE MOUNT ISA DEPOSIT

MOUNT ISA SILVER AND COBALT

ABSTRACT

The world class Mount Isa deposit, located within the Mount Isa Inlier, North West Queensland, contains deposits of copper, lead and zinc with ore genesis still contested. The copper orebodies are characterised by a relatively simple mineralogy of chalcopyrite, pyrite and pyrrhotite. Previous work on the sulphide assemblage of the Mount Isa copper ore bodies has identified significant accessory silver and cobalt. The mineralogy, paragenetic timing and mineral associations of these trace metals is still poorly defined. Samples from the 3500, 3000, 650 and 500 copper orebodies were investigated using optical petrology, SEM-EDS and MLA to identify and compare silver and cobalt-bearing minerals and textures. Monazites were also located for their potential to be analysed by U-Pb geochronology. LA-ICP MS was used to ascertain the relative abundances of trace elements within selected mineral species. A total of two cobalt-bearing minerals and four silver-bearing minerals were identified, including argentian chalcopyrite. Paragenetic observations results were consistent with findings from the lead-zinc orebodies at Mount Isa Mines. A monazite sample which had been previously found at Mount Isa Mines was dated to constrain paragenesis of mineralisation fluids which gave an age of 1614 ± 52 Ma, which correlates with the D₁ event in the Mount Isa inlier. Through the aforementioned methods, distribution of silver and cobalt trace metals throughout the Mount Isa copper system was determined to be heterogeneous and appears to be paragenetically comparable to the Pb-Zn lodes.

KEYWORDS

Mount Isa, silver, cobalt, mineralisation, trace element, LA-ICP-MS

TABLE OF CONTENTS

Title.....	i
Running Title.....	i
Abstract.....	i
Keywords.....	i
List of Figures and Tables	3
1. Introduction	4
2. Geological Setting and Background.....	5
2.1 Regional and local geology	5
2.3 Ore deposit geology.....	7
2.3 Cobalt	8
2.4 Silver.....	9
2.5 Ore genesis	10
2.6 Paragenesis	11
3. Methods	12
3.1 Sampling.....	12
3.2 Optical petrology	13
3.3 SEM/MLA	13
3.4 LA-ICP-MS	13
3.5 Data reduction.....	14
3.5.1 Trace elements.....	15
3.5.2 Geochronology	15
4. Observations and Results.....	15
4.1 Cobalt minerals.....	15
4.1.1 Petrology and SEM.....	15
4.1.2 MLA	18
4.1.3 LA-ICP-MS	20
4.2 Silver minerals.....	23
4.2.1 Petrology and SEM.....	23
4.2.2 MLA	26
4.2.3 LA-ICP-MS	27
4.2.4 Chalcopyrite	28
4.3 Monazite	30
4.3.1 Petrology and SEM.....	30

4.3.2 U-Pb monazite geochronology	32
5. Discussion	36
5.1 Cobalt	36
5.2 Silver.....	38
5.3 Monazite	39
6. Conclusions	42
7. Recommendations for further study	43
8. Acknowledgements	44
9. References	44
Appendix A: Laser parameters used at Adelaide Microscopy on LA-ICP-MS	48
Appendix B: Full petrology analysis of all 20 samples.....	48
Appendix C: LA-ICP-MS data	59
Appendix D: Silver assay data	60
Appendix E: Monazite locations	61

LIST OF FIGURES AND TABLES

Figure 1 Regional and geological map of the Mount Isa Inlier.....	6
Figure 2 Long section of the Mount Isa copper orebodies looking North-West.....	9
Figure 3 BSE images of cobalt-bearing minerals.....	17
Figure 4 MLA images of cobaltite and willyamite grains.....	19
Figure 5 ICP-MS elemental concentration maps from sample CLL-02.....	21
Figure 6 Scatter plots of various elemental concentrations of cobaltite.....	22
Figure 7 Petrological and BSE images of silver-bearing minerals.....	25
Figure 8 MLA image of galena vein	26
Figure 9 ICP-MS elemental concentration maps from sample RML-05.....	27
Figure 10 Scatter plots of various elemental concentrations of tetrahedrite	29
Figure 11 BSE images of monazite grains from the copper orebodies	31
Figure 12 BSE images of individual monazite grains	32
Figure 13 Sample 19CQ356DDR012 U-Pb Terra-Wasserberg Concordia plot.....	34
Figure 14 Sample 19CQ356DDR012 weighted average age plots	35

Tables

Table 1 Table showing the paragenesis of the Mount Isa copper orebodies.....	12
Table 2 DRS internal standards	15

1. INTRODUCTION

The world class Mount Isa copper-lead-zinc-silver (Cu-Pb-Zn-Ag) deposit is located within the Western Fold Belt of the Leichardt-River Trough of the Proterozoic Mount Isa Inlier, NW Queensland. Copper (Cu) ore bodies are characterised by a relatively simple mineralogy of chalcopyrite, pyrite and pyrrhotite. Previous work on the sulphide assemblage (Duckworth & Santaguida, 2009; Hinde, 1994; McGoldrick, 1986; painter, 2003) identified significant accessory silver (Ag) and cobalt (Co) within the Mount Isa copper system. The mineralogy, paragenetic timing and mineral associations of Ag and Co in this system is not defined at present and will be investigated in this study. By understanding the timing of mineralisation and spatial patterns of alteration and major/minor metal distribution throughout the deposit will allow us to predict their location in the crust and have a greater understanding of the volume and grade of the orebody. Mount Isa copper deposit contains complex spatial patterns of ore distribution which have been contested for several decades (Grondijs and Schouten, 1937; Murray, 1961; Perkins, 1984; Taylor and Lilly, 2016).

Recent advancements in LA-ICP MS techniques allow us to gather high-resolution trace elements and geochronological data in situ which will allow us to determine what Ag and Co-bearing minerals are present in the system, and to obtain an age for monazite in the system using U-Pb geochronology. By understanding the Mount Isa system as a single paragenetic event, a greater understanding of the relationship between the Cu and Pb-Zn lodes can be achieved. As economic resources become depleted, being able to identify low-grade ore zones within the varied Cu-Pb-Zn ore zones may assist multi-commodity mining in the area.

This study tests the following hypothesis:

1. Ag is only hosted by the mineral tetrahedrite
2. Co is only hosted by the mineral cobaltite
3. The distribution of Ag and Co is consistent between the copper orebodies investigated.

2. GEOLOGICAL SETTING AND BACKGROUND

2.1 Regional and Local Geology

The Mount Isa Cu-Pb-Zn-Ag deposit is located within the Mount Isa Inlier in North West Queensland, Australia (Figure 1). Deposited during the Proterozoic, the sediments are proposed to be the result of intracontinental rifting (Blake, 1987). The Mount Isa Inlier is divided into three sections, the Eastern Fold Belt, the Western Fold Belt and the central Kalkadoon-Leichardt Belt (Wilde, 2011). The Mount Isa deposit is situated in the Western Fold Belt in the Leichardt-river Trough, which is composed mainly of sedimentary and bimodal volcanic lithologies (Wilde, 2006). The Western Fold Belt has undergone several major tectonic events, one of the earliest resulting in the deformation and subsequent metamorphism of the 1900-1870 Ma basement rocks in the Barramundi Orogeny (Williams, 1998). The Isan Orogeny (1590-1500 Ma) terminated deposition and is associated with the majority of the regions mineralisation events (Betts and Lister, 2002) The Mount Isa Group, which hosts all economic mineralisation at the Mount Isa deposit, is comprised of carbonaceous shales and siltstones, deposited within an intra-continental basin (Neudert, 1983). The underlying basement is composed of meta-greenstone altered mafic volcanics and interbedded siliciclastic quartzite sediments of the Eastern Creek Volcanics (1710 ± 10 Ma) (Coaghan et al., 2003).

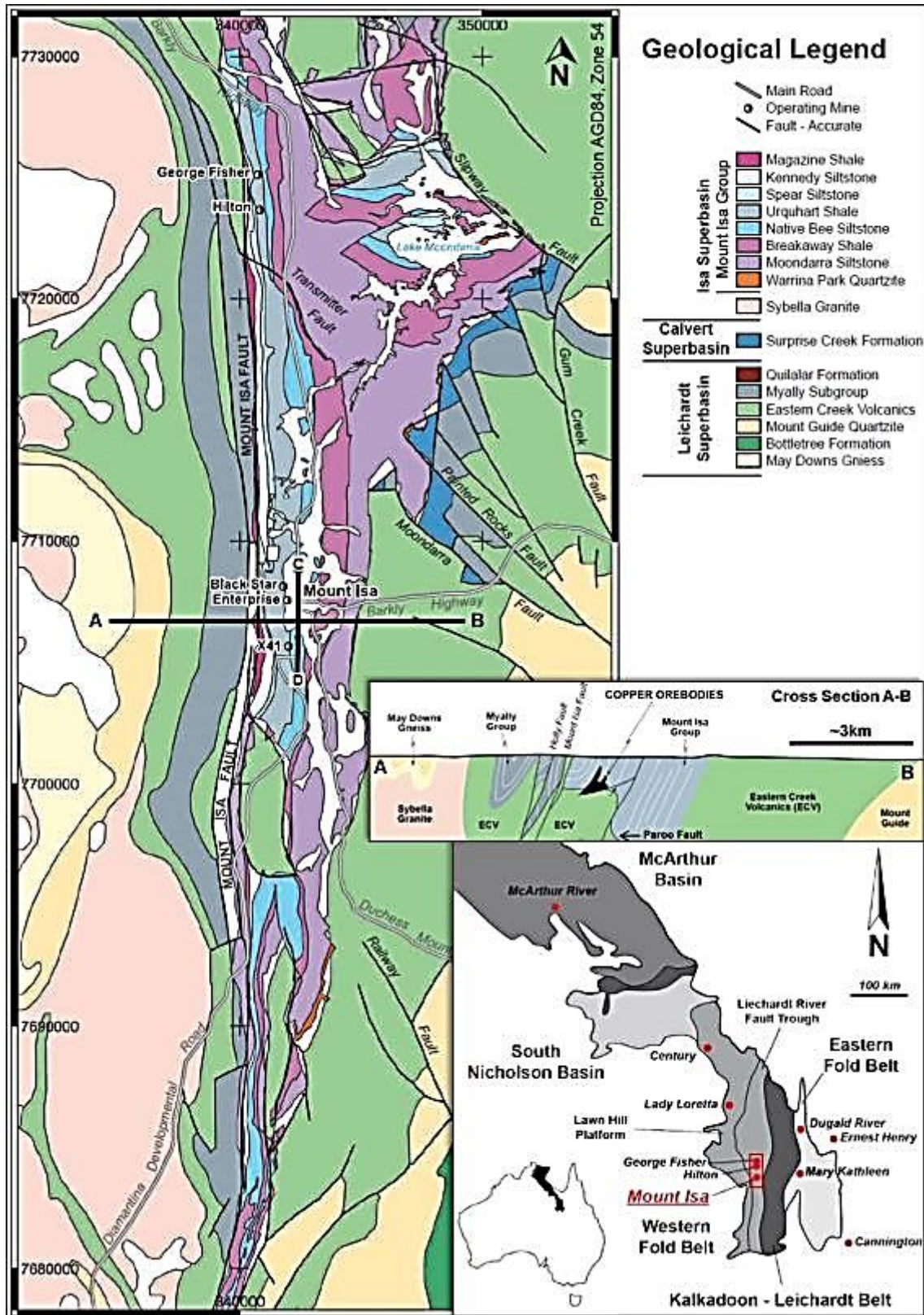


Figure 1: Regional Geology of the Mount Isa district, Mount Isa Inlier after Betts et al (2006) and Lilly et al (2017)

The Mount Isa Group contains the Warrina Park quartzite, Moondarra siltstone, Breakaway shale, Native Bee siltstone, Urquhart shale, Kennedy-Spear siltstone and the Magazine shale (Hinde, 1994). The Warrina Park Quartzite, Moondarra Siltstone and Breakaway shale are underlain by orthoquartzite and overlain by a siliceous shale unit (Blake, 1987). The aforementioned formations are generally comprised of dolomitic siltstones and small amounts of dolomite (Mathias and Clark 1975). Overlying these formations are the Native Bee siltstone, Urquhart shale, Kennedy-Spear siltstone and Magazine shale which are composed of tuffaceous dolomitic siltstones and shales (Mathias and Clark 1975). The ~1000 m thick Urquhardt Shale (1654 Ma \pm 4 Ma), which hosts all economic mineralisation at Mount Isa, is composed of variably siliceous and carbonaceous interbedded laminated and non-laminated siltstones and mudstones (Mathias and Clark, 1975).

Three major regional deformation events (D₁ to D₃) took place after deposition of the Mount Isa Group during the Isan Orogeny (1590 Ma to 1500 Ma), with copper mineralisation interpreted to have taken place between the D₂ and D₃ events (Perkins, 1984). The Mount Isa group has an unconformable faulted contact with the dominantly metabasaltic Eastern Creek Volcanics basement through the ramp structured Paroo Fault, which forms the lower contact of the major copper orebodies (Perkins, 1984).

2.3 Ore Deposit Geology

Eight major copper orebodies have been identified to date at Mount Isa (Painter, 2003). Copper mineralisation varies from massive to disseminated textures in the brecciated and altered Urquhardt Shales, (Painter, 2003) and is surrounded by a “silica dolomite” alteration halo (Mathias and Clark, 1975) which can extend up to several hundred metres beyond the copper mineralisation. The deepest orebody (3500) (Figure 2)

conforms to the flexure of the Paroo Fault and its contact with the Eastern Creek Volcanics (Perkins, 1990), indicating a possible route for hydrothermal fluid ingress (Miller, 2006). Sulphide minerals which have been identified in the copper system include pyrite, chalcopyrite, pyrrhotite and minor accessory cobaltite. Chalcopyrite is the only Cu-bearing mineral in the hypogene Mount Isa copper orebodies. Apatite, rutile, magnetite, orthoclase and rare monazite have also been recorded within the ore system, but have not been systematically investigated (Lilly et al, 2017).

2.3 Cobalt

Cobalt was first identified at Mount Isa copper deposit by Blanchard and Hall (1942) but at that point in time, the nature of the Co mineralogy was undetermined. Co was not investigated in the Mount Isa deposits before 1953 when Raynor (1953) commented on the presence of minor Co in the Broken Hill orebodies and how it may indicate the presence of Co within the Mount Isa orebodies. Croxford (1974) investigated Co at Mount Isa, identifying Co minerals cobaltite (CoAsS) alloclasite ((Co,Fe)AsS) from the 1100 and 3000 orebodies, respectively. Hinde (1994), briefly commented on the relationship between cobaltite and pyrite generations, also noting the grade of Co in relation to the copper orebodies. Hinde's work proposed that the Co grades were highest in the 3000/3500 followed by the 1100 orebody and hanging and footwall lenses. A report commissioned by Xstrata Copper (Duckworth and Santaguida, 2007) identified ferroan cobaltite ((Co,Fe)AsS), glaucodot ((Co,Fe)AsS), alloclasite ((Co,Fe)AsS) and cobaltian arsenopyrite (FeAsS) as the Co-As Fe phases in the MICO orebodies. Wilyamite ((Co,Ni)SbS) was also identified as a Co mineral which has an association with Sb and Ni. According to a report by the Geological Survey of Queensland (2014), the Mount Isa orebodies combined contain ~0.14% Co. Refining of sulphides is able to

recover <1000 tonnes of Co per annum, however, ~10,000 tonnes per annum (tpa) of Co is discarded in tailings because of its association with pyrite (FeS_2).

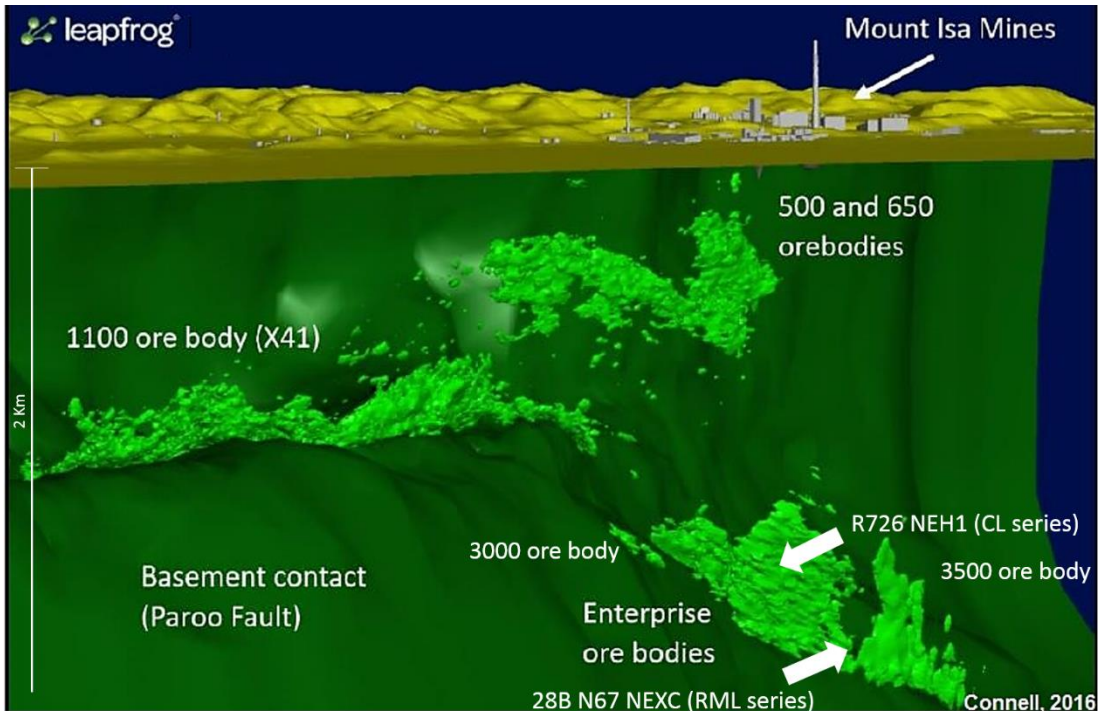


Figure 2: Cross-section of the Mount Isa copper orebodies looking North-West. The approximate location of thesis sample thin sections are highlighted. Adapted from Connell (2016). Note; orebodies numerical names are based on their depth from surface on a mine grid.

2.4 Silver

Silver has not been extensively studied in the copper orebodies at Mount Isa because of the close proximity of Pb-Zn-Ag ore system directly adjacent. The majority of studies have been conducted within the Mount Isa Pb-Zn-Ag deposit. Ag was initially identified by Grondijs and Schouten (1937) in samples from the Black Star mine, occurring as Ag rich tetrahedrite ($\text{Ag}_{10}(\text{Fe},\text{Zn})_2\text{Sb}_4\text{S}_{13}$), polybasite $[(\text{Ag},\text{Cu})_6(\text{Sb},\text{As})_2\text{S}_7][\text{Ag}_9\text{CuS}_4]$ and occasionally proustite (Ag_3AsS_3). This initial work has been supported by additional research (Blanchard and Hall, 1942; Harris et al 1984 Painter, 2003). Blanchard and Hall (1942) determined that based on average Ag content in samples, it is considered

argentotetrahedrite (Ag-rich tetrahedrite) is the main Ag-bearing mineral in the Mount Isa Pb-Zn-Ag system as opposed to freibergite $(\text{Ag,Cu,Fe})_{12}(\text{Sb,As})_4\text{S}_{13}$, which is supported by Riley (1974) who assayed samples from the Pb-Zn-Ag orebody with a range of 18.4 to 42.5 wt. % Ag. Supergene native Ag in leaf and wire form has been identified in the Pb-Zn-Ag deposit at depths of up to 150ft (Blanchard and Hall, 1942).

2.5 Ore genesis

The original epigenetic mineralisation model was introduced by Grondijs and Schouten (1937) which proposed that all Cu-Pb-Zn-Ag ore was epigenetic and co-eval. The paradigm was that shales were hydrothermally replaced in selected beds of galena, sphalerite and pyrite with breccia-hosted chalcopyrite (eg. Blanchard and Hall, 1942; Stillwell and Edwards, 1945; Schouten, 1946; Knight, 1957; and Carter, 1953).

Later work by authors including Fisher (1960) and Murray (1961) advocated a theory of cogeneration of the two separate sediment hosted deposits (Pb-Zn-Ag and Cu) with a syngenetic origin. The Cu orebodies were proposed to have been recrystallised and remobilised during orogenesis to further support this particular model. Perkins (1984) proposed a syngenetic sediment hosted Pb-Zn-Ag system with epigenetic copper mineralisation, which incorporated Cu-bearing brines entering the Urquhart shale during the D₃ deformation event. Perkins model was supported by work of Swager (1985) and Bell et al. (1988), however the mechanism of emplacement remained controversial. Continued work by Perkins (1997) resulted in a revised theory advocating a single epigenetic hydrothermal event that coevally formed the Cu and Pb-Zn-Ag orebodies, consistent with the original work by Grondijs and Schouten (1937).

More recently, a review of all models was conducted by Taylor and Lilly (2016) with additional paragenetic studies. The study concluded that all sulphides belong to the same deformation stage (Taylor and Lilly, 2016), supporting the original observations by Grondjjs and Schouten (1937). At present, evidence suggests that Mount Isa is a zoned carbonate replacement system (Taylor and Lilly 2016, Lilly, 2017) and the origin is consistent with the epigenetic model proposed by Gulson (1983) and Perkins (1997).

2.6 Paragenesis

The paragenesis and relative timing of the Mount Isa copper system has been studied extensively (e.g. Perkins 1990; Painter 2003; Wilde 2006) to determine the relative timing and formation of the Mount Isa system (Table 1). The most recent paragenetic review was conducted by Taylor (2016) (Table 1). The paragenesis can be simplified into 5 distinct stages. Relative timing of Ag and Co minerals in the copper deposit, and how they relate to the main sulphide stage have not been described in detail.

- Stages 1 and 2 (pre-ore) consisted of enriched chlorite infill/alteration followed by quartz veins which contained minor infill textures within the Eastern Creek Volcanics basement contact.
- Stage 3 (pre-ore) included the initial deposition of fine grained pyrite (pyrite 1).
- Stage 4 (main ore stage) is proposed as a prolonged hydrothermal event which introduced silica-dolomite during the earlier stages and subsequently introduced economic sulphides during a brittle fracture event. A reduced sulphur fluid is believed to have facilitated the precipitation of the economic mineralisation (Perkins, 1997), which were also constrained by impermeable bedding and

structures during Pb-Zn deposition. Perkins (1997) also implies that chalcopyrite was the youngest sulphide deposited based on temperature controlled zonation.

- Stage 5 was the final stage identified, which resulted in variable chloritisation overprinting of previous paragenetic stages (Taylor, 2016)

Table 1: Paragenesis of the different mineralisation stages at the Mt Isa Cu-Pb-Zn-Ag deposit adapted from Maguire (2016).

	Stage 1	Stage 2	Stage 3	Stage 4	Stage 5
Chlorite	Green oval				Green oval
Quartz		Grey oval		Grey oval	
Pyrite 1			Yellow oval		
Carbonate-1 ± quartz ± pyrite 2 ± cobaltite				Blue oval	
Carbonate-2 ± minor sericite				Pink oval	
Chalcopyrite, sphalerite ± galena ± pyrrhotite ± minor carbonate ± arsenopyrite ± tetrahedrite				Orange oval	

3. METHODS

3.1 Sampling

Fieldwork was conducted at Mount Isa Copper Operations (MICO), in February-March 2017. Chalcopyrite-bearing samples were collected from diamond drill hole number 201604012, located at Level 32A; R726 NEH1 of the Copper deposit (127.4-127.7 m). Thin sections were also made from hand samples collected from the 28B N67 NEXC location which links the 3000 and 3500 orebodies (Figure 2). All polished thin sections were made by Ingham Petrographics, QLD.

Historical samples from the Mount Isa 650 and 500 orebodies were selected from the economic geology collection at the University of Adelaide. Samples were selected based on their high abundance of chalcopyrite, galena and pyrrhotite.

3.2 Optical Petrology

Optical microscopy was used to conduct petrology on the thin section samples using the Olympus DP21 Camera, the Olympus BX51 microscope and Olympus TH4-200 light source. Reflected light microscopy was used to identify different sulphide minerals and potential Ag and Co-bearing minerals.

3.3 SEM/MLA

The Scanning Electron Microscope (SEM), FEI Quanta 600 Mineral Liberation Analysis (MLA) was used to generate high resolution trace mineral maps of each sample. The investigation focused on locating Ag and Co-bearing minerals as well as other identified trace minerals including monazite and rutile. Backscatter election (BSE) maps were created using a solid-state BSE detector which generated mean atomic number imaging as well as a thin detector to generate X-ray analysis.

Energy dispersive X-ray analysis (EDS) was used to determine the mineralogy present in samples. Highly reflective minerals were targeted due to sulphides having a larger greyscale number when compared to gangue minerals (calcite, quartz, silica-dolomite).

When a grain of interest was identified, it was recorded for subsequent laser ablation to determine its chemical composition. Brightness and contrast parameters were also adjusted to assist in identifying less distinguishing minerals or minerals with similar greyscale.

3.4 LA-ICP-MS

Laser ablation was conducted on four thin sections to investigate the relative abundances of Co and Ag. Minerals pyrite, chalcopyrite, cobaltite, tetrahedrite, boulangerite and galena were ablated, full datasets can be found in Appendix C.

Agilent 7700 ICP-MS with attached 193nm RESOLUTION LR Excimer Laser

Laser Ablation-Inductively Coupled Plasma-Mass Spectrometry (LA-ICP-MS) was used on 4 of the Mount Isa thin sections (CL-02, CL-03, RL-02, RL-05) to determine the trace element composition of specific sulphides. MASS-1 powdered sulphide and GSD basaltic glass standards were used on chalcopyrite, pyrite, cobaltite, tetrahedrite, boulangerite and galena to determine geochemical variation within grains.

Agilent 7500s with attached ASI M-50 laser ablation system

ASI M-50 laser ablation system MADEL, 222 and Ambat monazite standards were used on two monazites in sample 19CQ356DDR012 to determine in situ U-Pb geochronology. A small 9µm spot size was used because of the irregular shape of the monazites. Only U-Pb geochronology elements (U^{238} , Pb^{206} , Pb^{207} , Hg^{204} , Pb^{204}) were used analysed due to trace analysis resulting in an increased error range.

3.5 Data Reduction

3.5.1 Trace elements

The trace element maps of Co and Ag-bearing grains were generated with Iolite software (Paton et al., 2011). Trace Element IS data reduction scheme (DRS) was used to determine the trace element compositions of analyses using the following internal standards.

Table 2: Trace element data reduction scheme internal standards used for analysed minerals

<i>Mineral</i>	<i>Element</i>	<i>Internal standard (wt %)</i>
<i>Pyrite</i>	Fe	46.5
<i>Chalcopyrite</i>	Fe	30.4
<i>Cobaltite</i>	As	45.16
<i>Tetrahedrite</i>	Cu	34.80
<i>Boulangerite</i>	Pb	54.88
<i>Galena</i>	Pb	86.60

3.5.2 Geochronology

Iolite (Paton et al., 2011) was used to generate a $^{207}\text{U}/^{206}\text{Pb}$ corrected age, while correcting for instrumental drift and error in analyses. Adelaide Microscopy monazite standard (MAdeI) was the primary standard used with standards 222, and Ambat used to ensure accuracy. Laser analyses which displayed poor signals or did not display acceptable monazite peaks were not included in age calculations. Isoplot (Ludwig, 2003) was used to construct Terra-Wasserberg plots for monazite and generated ^{207}Pb corrected overall $^{238}\text{U}/^{206}\text{Pb}$ weighted mean ages for monazite grains, as well as individual ages.

4. OBSERVATIONS AND RESULTS

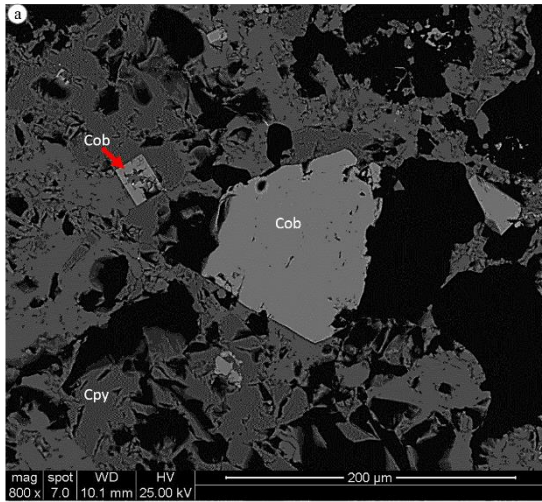
4.1 Cobalt minerals

4.1.1 Petrology and SEM

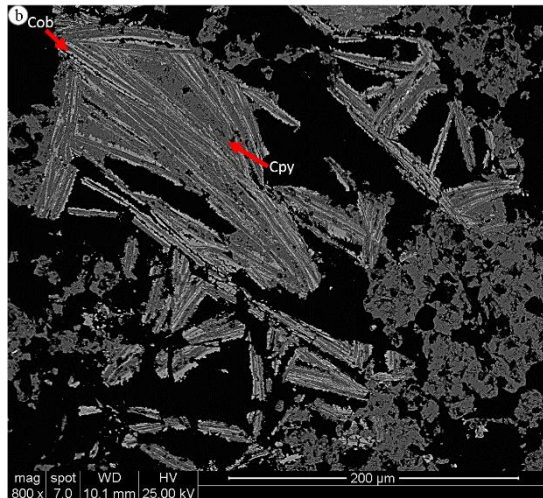
Cobalt-bearing minerals are very difficult to discriminate using optical petrology, so minerals such as pyrite, chalcopyrite and galena were identified through optical petrology before further investigation using SEM EDS. During SEM EDS analysis the sulphide minerals cobaltite and willyamite were observed in samples from the 3500 orebody and in historical samples from the 500 and 650 orebodies. Co is not distributed

homogenously throughout the samples, with CL series samples (3500 orebody) and historical samples (500 and 650 orebodies) containing a higher abundance of cobaltite to that of RL series samples (3000 orebody). A total of 14 polished blocks and thin sections were investigated under SEM to determine the presence of Co. Using energy dispersive X-ray analysis, six samples (CLL-01, CLL-02, CLL-03, 6055, 6110, 6086) were determined to contain Co-bearing minerals. The size of cobalt-bearing grains ranged from ~10-300 μ m. Co-bearing minerals form as acicular, cubic, or replacement textures in close association with pyrite (Figure. 3). Petrology of all thesis samples can be found in Appendix B.

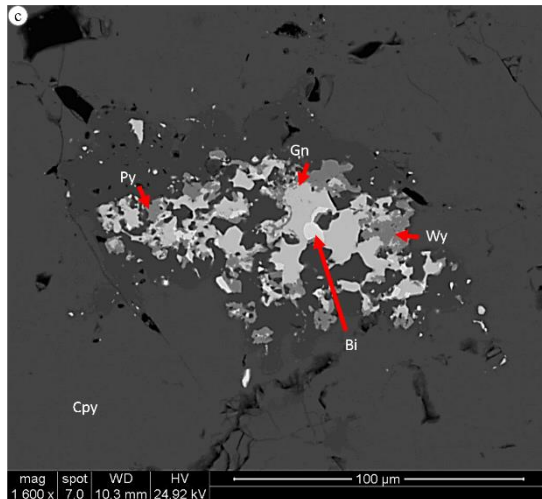
Cobaltite (CoAsS) has been observed to have encircled the original framboidal structure of pyrite 1, indicating that cobaltite precipitated after pyrite 1. Cobaltite was also observed texturally associated with chalcopyrite and non-sulphide gangue minerals including quartz and silica-dolomite (Figure 3). Willyamite ((Co, Ni) SbS) was identified in sample CLL-03, located within chalcopyrite, with associated galena, pyrite and trace amounts of native bismuth (Fig. 3c). Auxiliary trace minerals identified as individual grains associated with Co minerals included acanthite (Ag₂S), brannerite ((U,Ca,Ce)(Ti,Fe)₂O₆), monazite (Ce, La, Nd, Th)PO₄, and ullmannite (NiSbS), the nickel rich end member of the willyamite solid solution series.



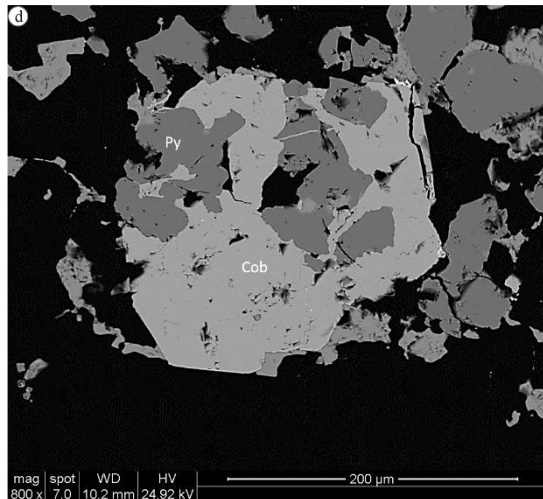
Sample CLL-01: Large Cobaltite (cob) grain within chalcopyrite (cpy) displaying sub-euhedral cubic textures



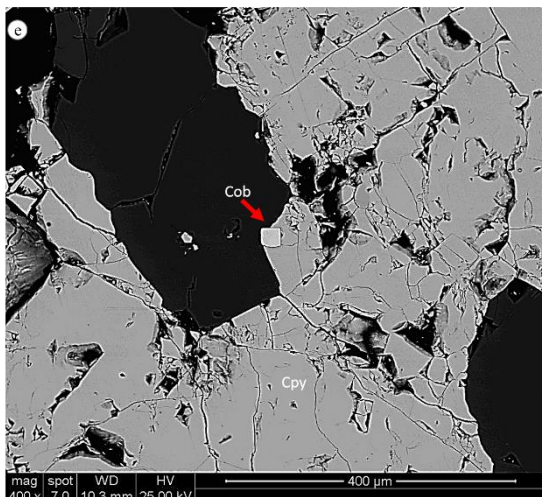
Sample CLL-02: Cobaltite (cob) with chalcopyrite (cpy) in an interlacing acicular intergrowth texture with chalcopyrite appearing to replace cobaltite



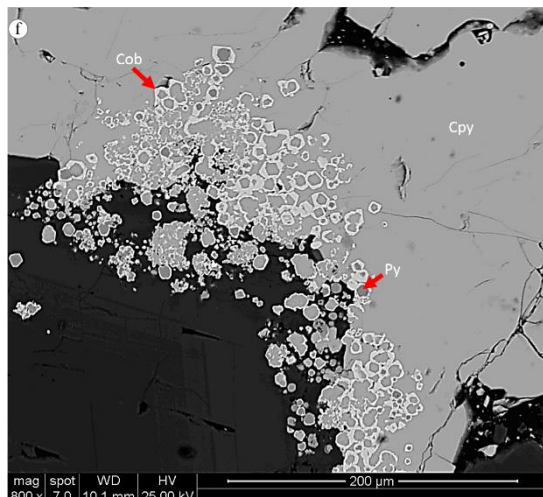
Sample CLL-03: anhedral grain with willyamite (wy), pyrite (py), galena (gn) and trace amounts of bismuth (bi) within chalcopyrite



Sample CLL-03: Euhedral cobaltite (cob) infilling around and replacing pyrite 1 (py)



Sample 6110: Small euhedral cobaltite grain (cob) at contact between chalcopyrite (cpy) and quartz



Sample 6086: Cobaltite (cob) overgrowing framboidal pyrite 1 (py) with chalcopyrite (cpy) overgrowing cobaltite at contact between chalcopyrite and silica-dolomite

Figure 3: BSE images of cobalt minerals located in the following mine locations (a, b, c, d) 3500 orebody, (e and f) 650 orebody

4.1.2 MLA

MLA analysis supports optical and SEM observations that cobaltite forms “atoll” structures with pyrite 1, where cobaltite encircles framboidal grains of pyrite (Figure 3f). Other Co-bearing minerals distinguished by MLA include cobaltian arsenopyrite, ullmannite, and willyamite (Figure 3c). However, the limitations of MLA made it difficult to distinguish between willyamite and cobaltian ullmannite. MLA confirmed that Co-bearing minerals identified in aggregate grains of sample CLL-03 were not cobaltite but antimony-rich willyamite (Figure 4). MLA was able to positively identify grains of interlacing cobaltite and chalcopyrite (figure 4a). All non-cobaltite Co-bearing minerals were observed within chalcopyrite in aggregates with pyrite and galena, with trace metal native bismuth also present (Figure 3c).

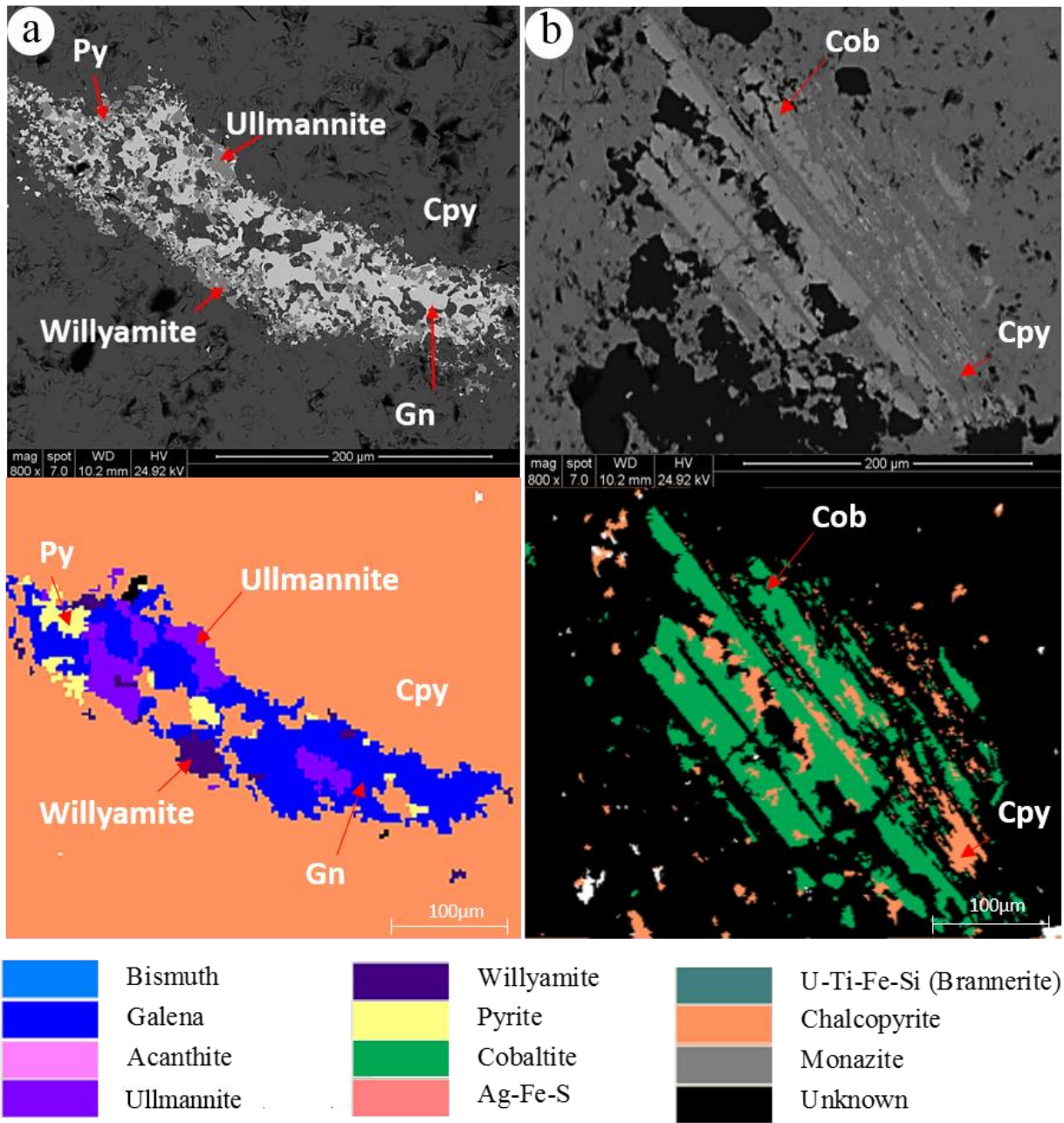


Figure 4: BSE images of trace element grain and mineral liberation analysis maps of Co-bearing minerals willyamite (a) showing clear differentiation between solid solution series Ni rich ullmanite and Co rich willyamite and cobaltite (cob) (b), with MLA image indicating possible elemental variation in chalcopyrite

4.1.3 LA-ICP-MS

Two chalcopyrite-cobaltite laser maps were generated from samples CLL-02 and CLL-03 (Figure 5). Because these grains were relatively small, the spot sizes had to also be small (7 and 10 μ m respectively); the laser map from sample CLL-02 was the only map that was able to be analysed successfully (Figure 5). The area imaged contained inter-fingering grains of cobaltite and chalcopyrite which were initially observed in MLA imaging (Figure 3b and 4b). The top-right-hand-corner of the scan has elevated As, Co, Bi, Ni which could indicate that there are inclusions native Bi in chalcopyrite which would be consistent with previous observations (Figure 3c).

Laser ablation analysis determined cobaltite has an average Co concentration of 33.6%, less than its ideal chemical composition of 35.52% Co. Chalcopyrite has Co concentrations of up to 3.7%. Figure 6 displays the major element variation within the cobaltite samples. Cobaltite has a mean of 460ppm Cu, indicating that Cu can substitute into the crystal lattice of cobaltite and may substitute inversely in chalcopyrite (Huston, 1995). Cobaltite analyses had up to 5.8% Cu, which has been attributed to contamination of chalcopyrite inclusions supported by the poor correlation observed in figure 6c. While the abundance of Co is generally consistent throughout samples CLL-02 and CLL-03, the abundance of nickel ranges from 0.14% to 2%. In cobaltite samples, there was a moderate negative correlation between Co and Fe (Figure 6a).

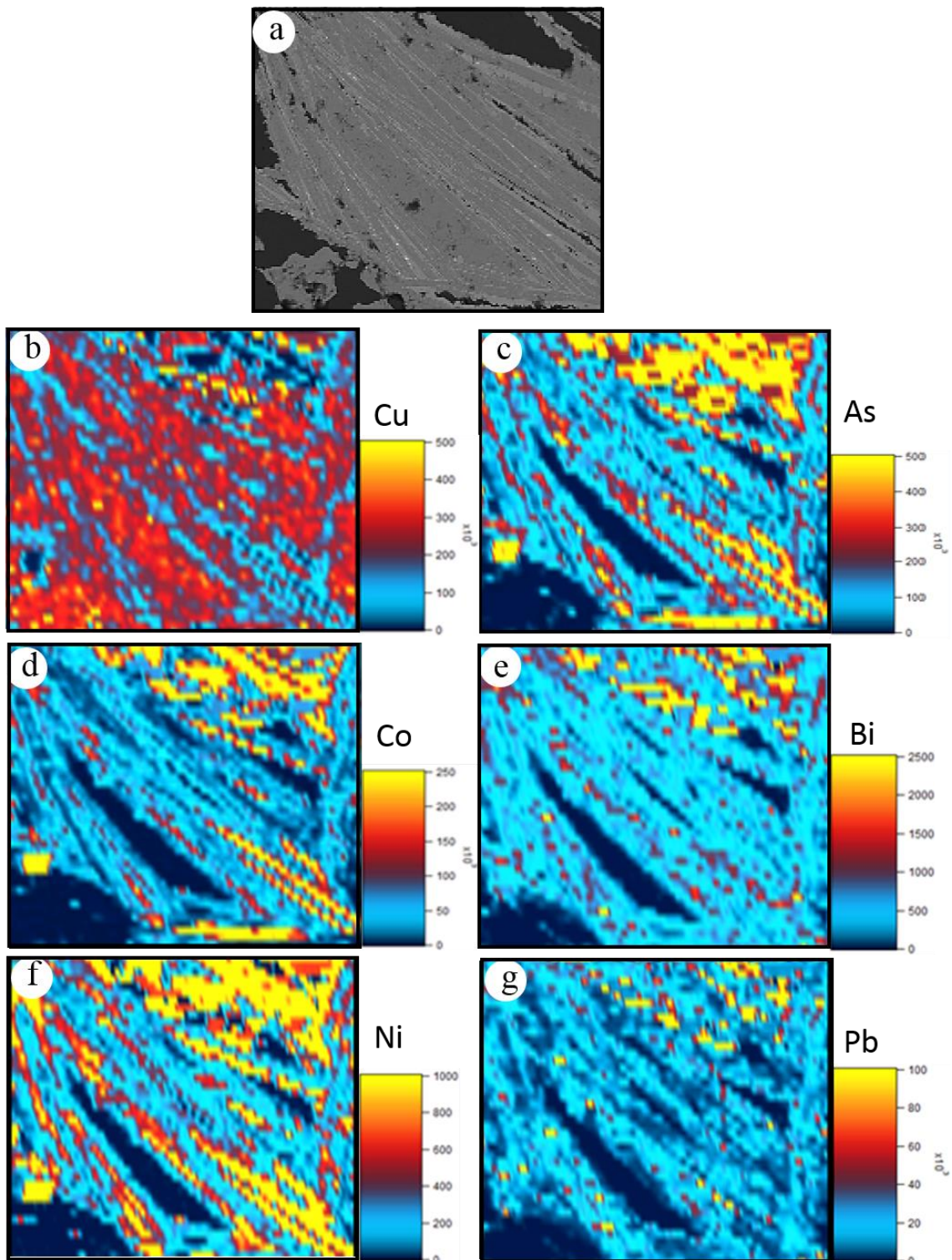


Figure 5: Laser maps of interlacing cobaltite and chalcopyrite from thin section sample CLL-02: a) SEM image ... b-g) the different elements mapped. Note the inter-fingering of chalcopyrite and cobaltite grains.

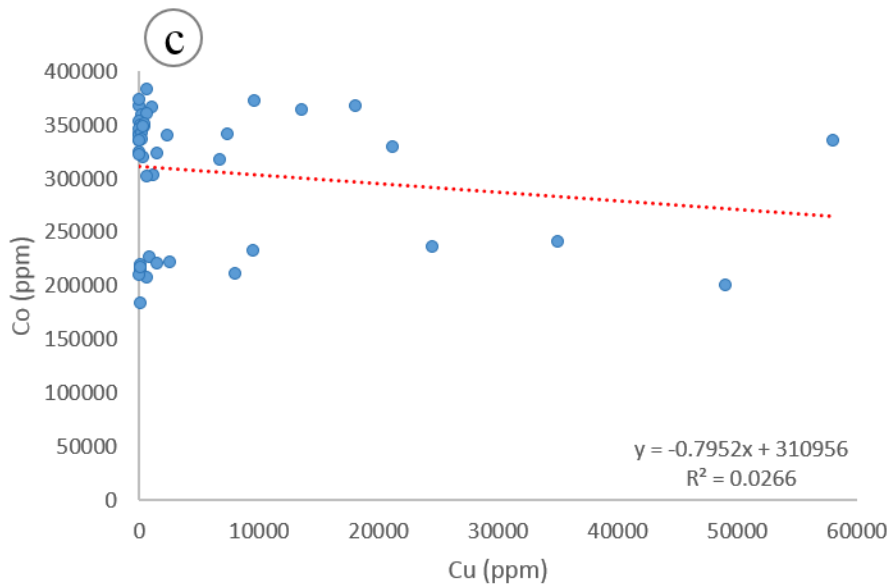
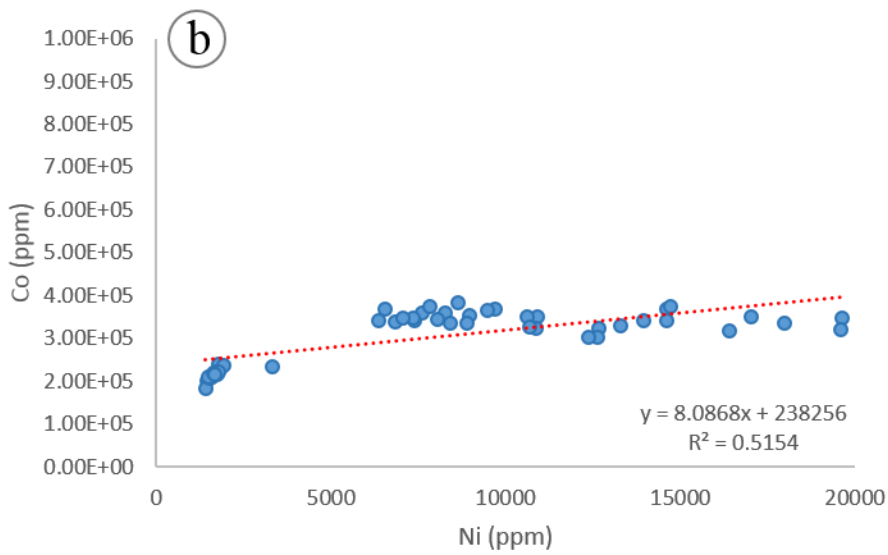
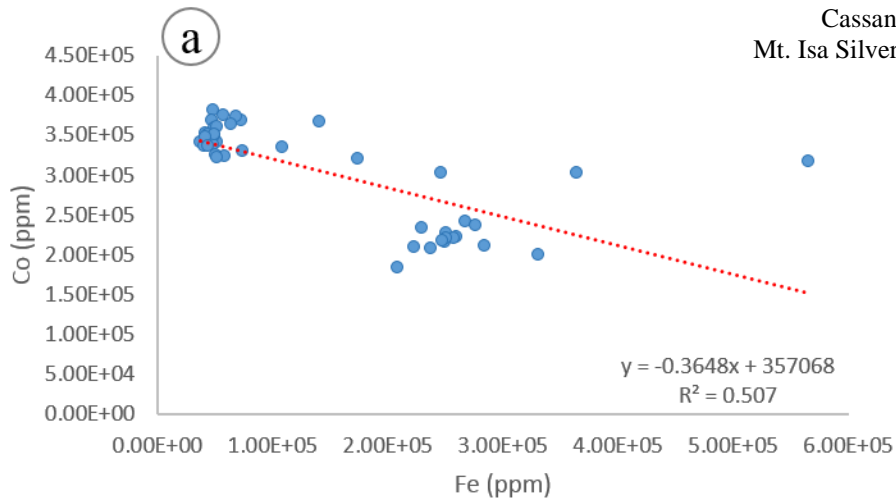


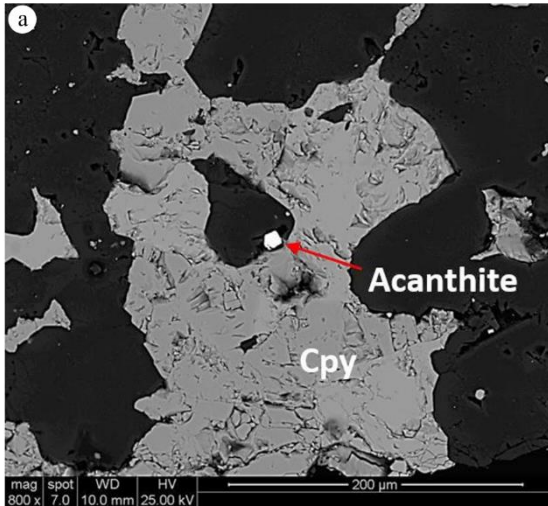
Figure 6: Scatter plots showing abundance and correlations of various elements relative to Co. (a) Co vs. Fe; (b) Co vs. Ni; and (c) Co vs. Cu

4.2 Silver minerals

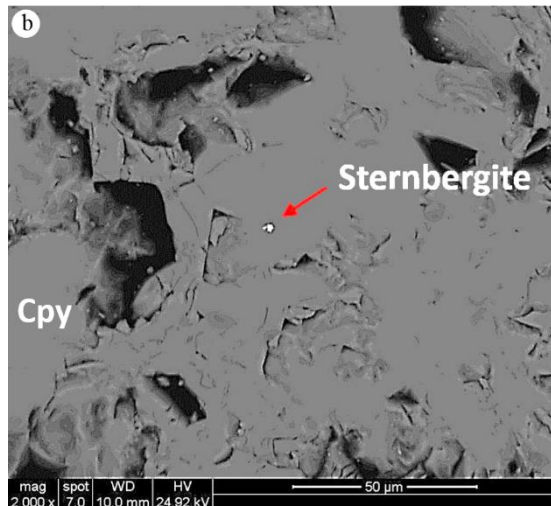
4.2.1 Petrology and SEM

Ag-bearing minerals were located in samples 6084, 6085, CLL-01, RML-02, RML-03 and RML-05 (Figure 7). Size of Ag-bearing minerals ranged from ~4-200 μ m. Ag mineralogy was observed in samples collected between the 3000 and 3500 orebodies and in historical samples from the 650 orebody. Four grab samples collected from the 28B N67 NEXC used to generate the RL series samples were highly enriched in Ag-bearing sulphides and contained up to 696ppm Ag with 40% Pb (full data set in Appendix D). Differentiation nomenclature used by Riley (1974) was implemented for this study, where Ag values below 20wt% are argentian tetrahedrite and those above are freibergite, as the distinction between freibergite and tetrahedrite is not clearly defined. Argentian tetrahedrite ($\text{Ag}_{10}(\text{Fe,Zn})_2\text{Sb}_4\text{S}_{13}$) was identified in samples in exclusive association with galena and the antimony-lead sulphosalt boulangerite ($\text{Pb}_5\text{Sb}_4\text{S}_{11}$), with a coeval anhedral texture between tetrahedrite and boulangerite (Figure 7 c,d,e,f). Tetrahedrite and boulangerite appear to co-exist within galena. However, individual grains of boulangerite were observed within galena veins (Figure 7e). Tetrahedrite appears to preferentially precipitate within veins of galena as an inclusion but was also observed in contact with chalcopyrite, quartz and other non-sulphides such as silica dolomite. Sulphate minerals, arsenopyrite (FeAsS) and gudmundite (FeSbS) were also observed using the SEM EDS, however were not investigated further as they were not part of the scope for this study. Optical petrology and SEM EDS results are analogous to previous work completed on the Mount Isa Pb-Zn-Ag orebody by Riley (1974). SEM EDS analysis of Ag-bearing minerals confirmed petrographic observations of the presence of boulangerite and tetrahedrite. Acanthite (Ag_2S) (Figure 7a) and sternbergite

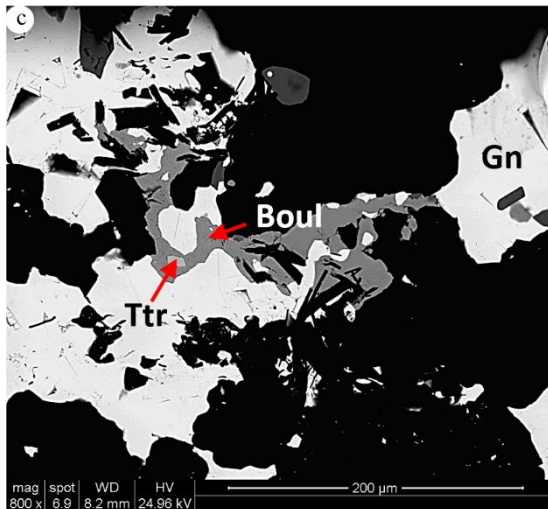
(AgFe_2S_3) (Figure 7b) were also observed as singular grains with euhedral textures in the 650 and 3500 orebodies.



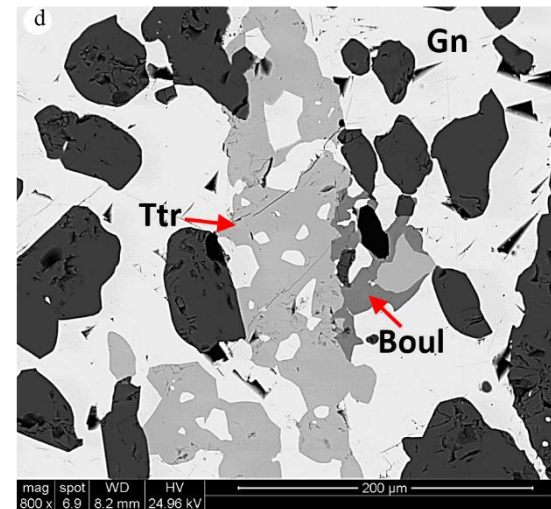
Sample 6085: Acanthite grain at boundary between chalcopyrite (cpy) and quartz



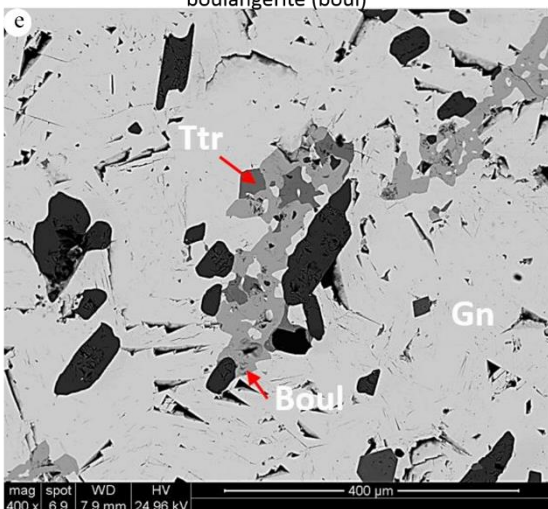
Sample CLL-01: Sternbergite grain within chalcopyrite (cpy) mass



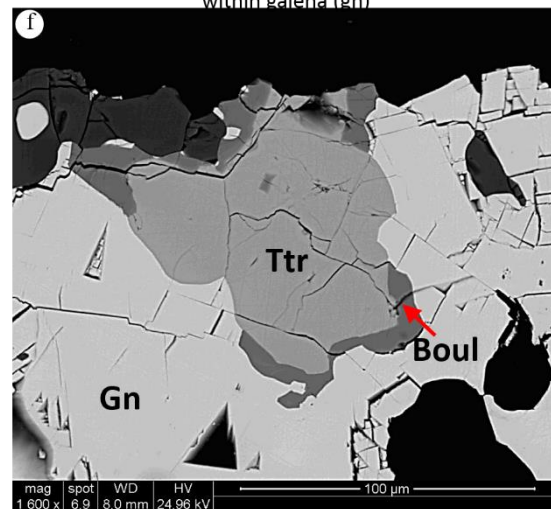
Sample RML-03: Tetrahedrite (ttr) enclosed within boulangerite (boul)



Sample RML-04: tetrahedrite (ttr) and boulangerite (boul) within galena (gn)



Sample RML-05: tetrahedrite (ttr) and boulangerite (boul) within galena (gal)



Sample RML-05: large tetrahedrite (ttr) grain with boulangerite (boul) on edges of grain within galena (gn)

Figure 7: BSE images of silver mineral located in the following mine locations (a) V30 East Decline, 11/L 809, (b-f) 28B N67 NEXC (link between 3000/3500 orebodies)

4.2.2 MLA

MLA supports petrographic and SEM EDS analyses that tetrahedrite and boulangerite are geochemically distinct from one another based on an abundance of Ag in tetrahedrite and Pb present in boulangerite (Figure 8). Both sulphosalts regularly display an anhedral co-precipitated texture which is congruous with observations from the Mount Isa Pb-Zn-Ag orebody (Riley, 1974). MLA parameters were set to classify minerals with >70% confidence on the X-ray spectra, therefore MLA was unable to correctly identify all mineral species (see figure 4b).

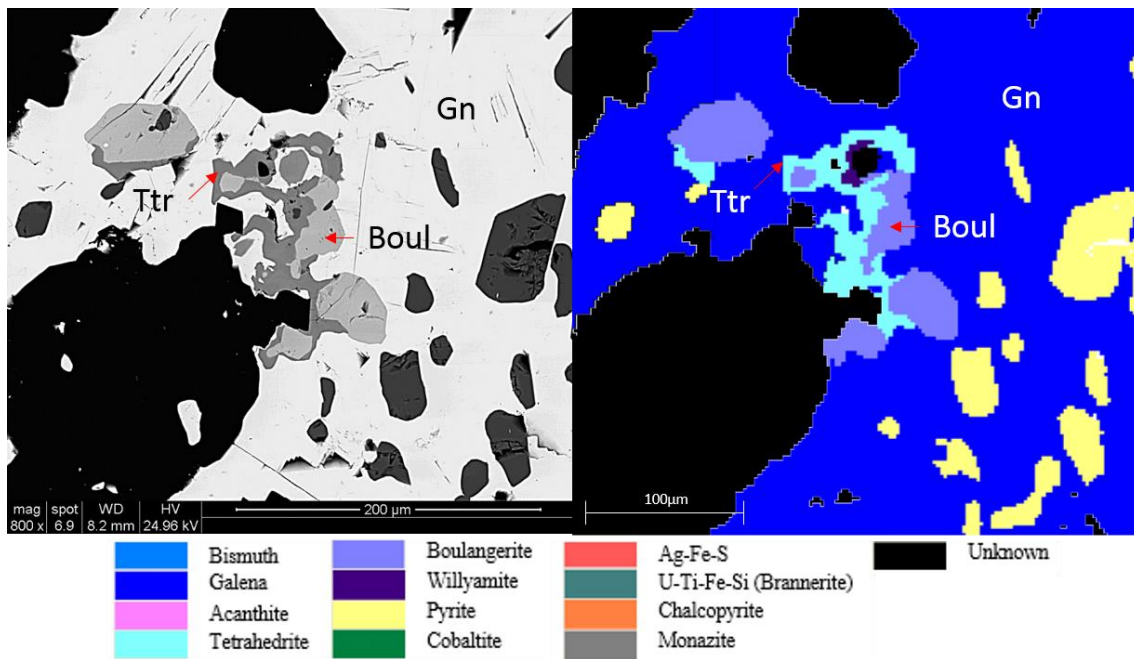


Figure 8: MLA images of trace element grain and mineral liberation analysis maps of Ag-bearing mineral tetrahedrite (Ttr) and associate Ag absent mineral boulangerite (Boul) within galena (Gal).

4.2.3 LA-ICP-MS

Elemental maps were produced for two Ag-bearing grains on samples RML-02 and RML-05 (Figure 9) using a 7 μ m spot size, which generated poor analyses and low quality map images. Laser maps confirmed a geochemical variance between tetrahedrite and boulangerite, in particular sulphur variation. Tetrahedrite has a stoichiometric sulphur concentration of 25.37% compared to that of boulangerite at 18.68%. Analyses showed an average Ag content of 10.35% in tetrahedrite, which is marginally lower but within error of the minimal content in Ag-rich tetrahedrite of 10.65% (Kolodziejczyk, 2016).

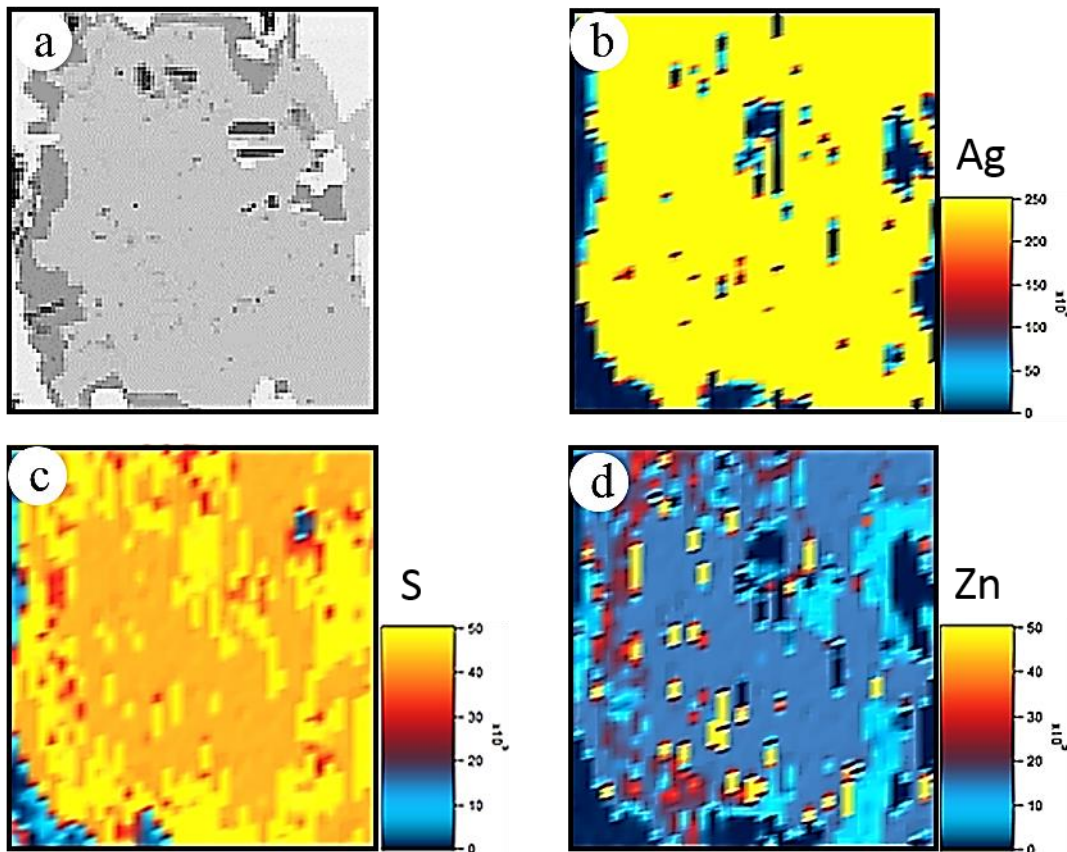


Figure 9: Laser maps of Ag-bearing tetrahedrite and boulangerite from sample RML-05. Note in particular the variation of sulphur between tetrahedrite and boulangerite

4.2.4 CHALCOPYRITE

To investigate the potential of Ag as micro-inclusions or as solid-solution within chalcopyrite, as noted by Riley (1974), samples CLL-02 and CLL-03 were analysed by LA-ICP-MS. 31 spot analyses of chalcopyrite measured Ag concentration from 35.8 ppm to 3.9%, with an average Ag content of 182.2ppm. Bivariate scatter plots of chalcopyrite data (Figure 10) indicates there is a strong positive correlation ($R^2 = 0.83$) between Cu and Ag concentrations in chalcopyrite in these samples (Figure 10a). Zn within chalcopyrite had an average count of 463ppm, with a similar positive correlation ($R^2 = 0.73$) to that of Cu (Figure 10f). This indicates that there may be an elemental relationship between Ag, Cu and Zn within chalcopyrite. This is supported by work by Head (2007) which indicated there is a weak correlation between Cu and Ag in the central zone, where RML series (3000 orebody) samples were located (figure 2).

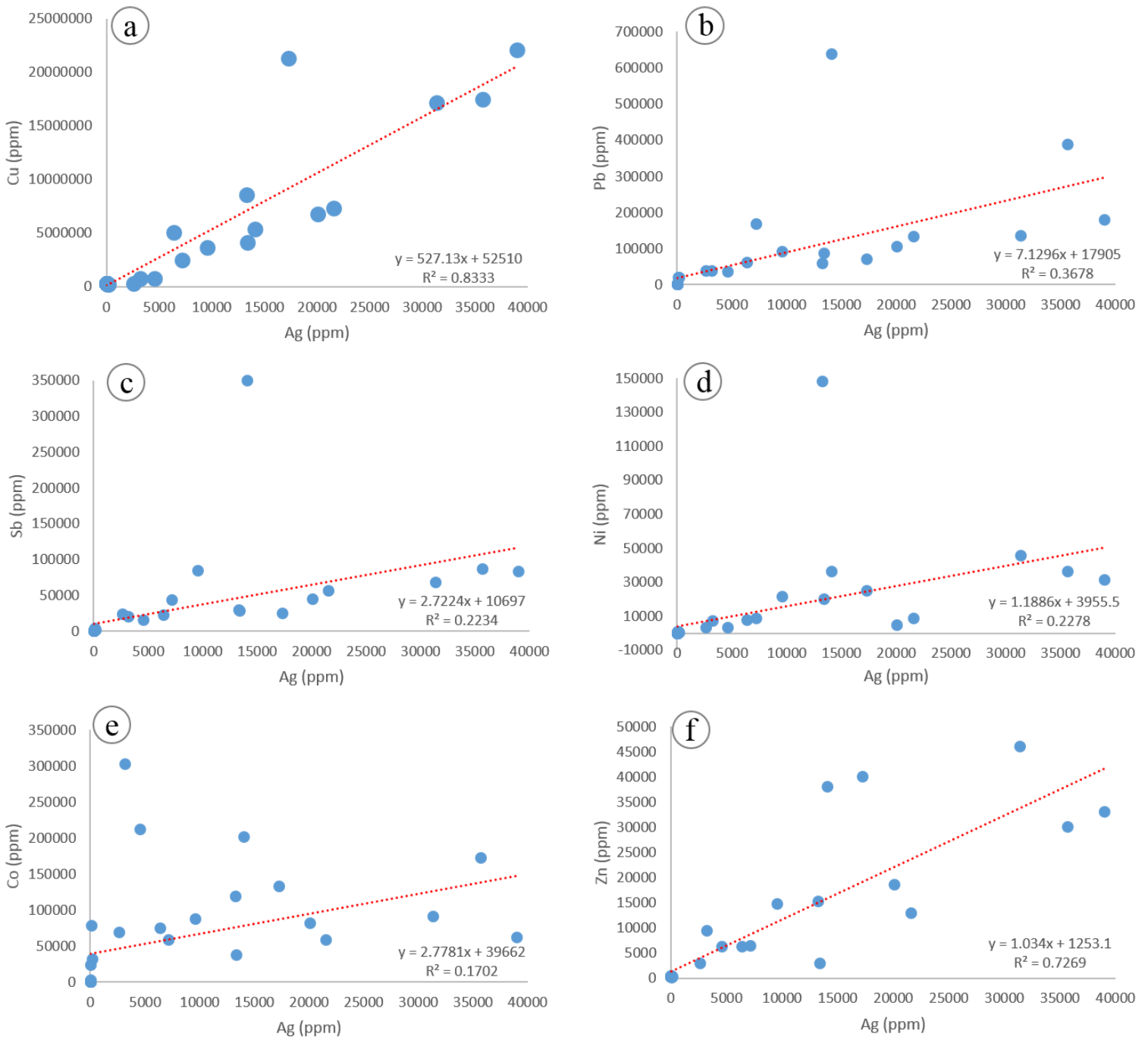
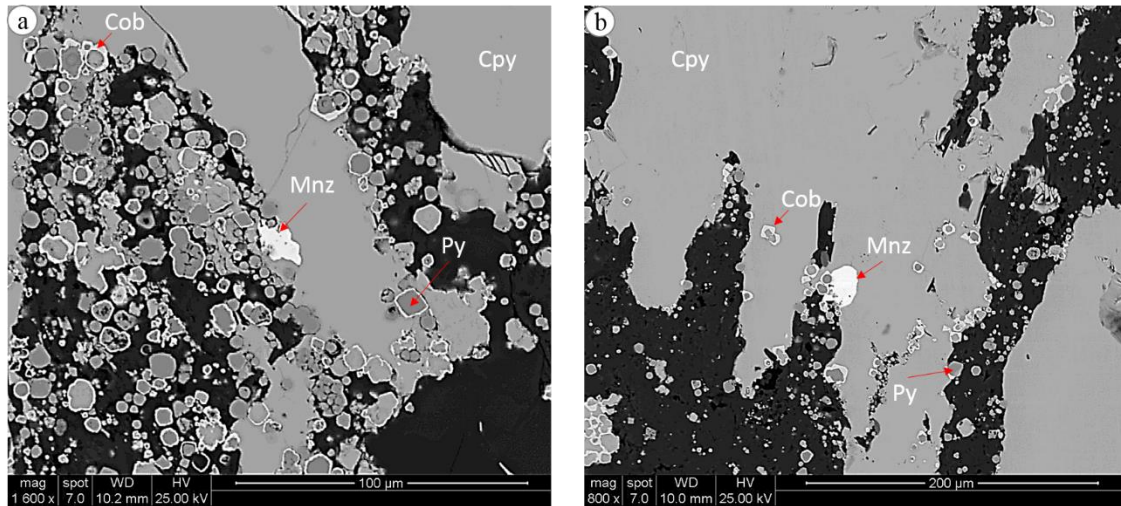


Figure 10: Scatter plots showing abundance and correlations of various elements relative to silver in chalcopyrite. (a) Ag vs. Cu; (b) Ag vs. Pb; (c) Ag vs. Sb; (d) Ag vs. Ni; (e) Ag vs. Co and (f) Ag vs. Zn with n=31

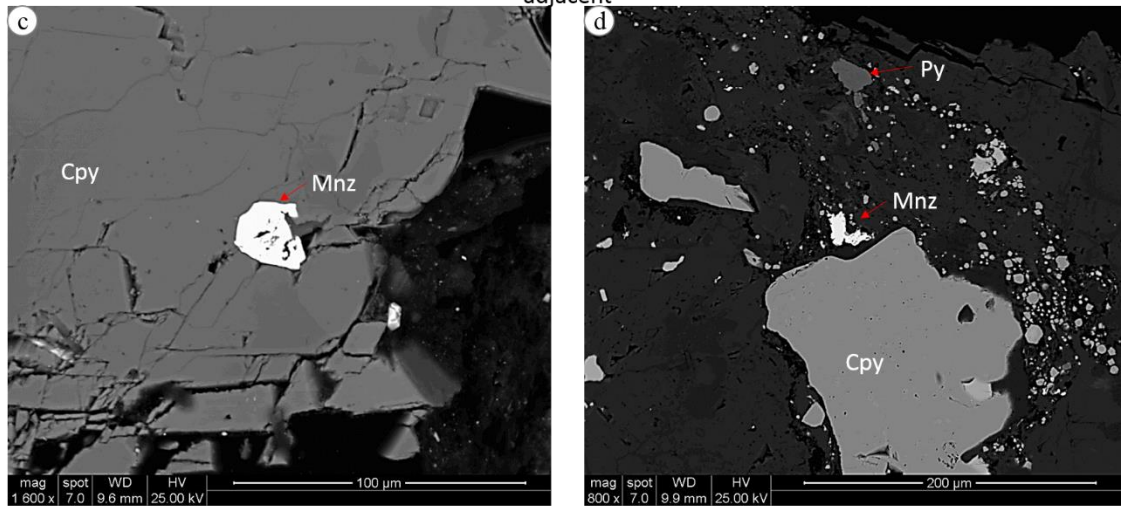
4.3 Monazite

4.3.1 Petrology and SEM

A total of 26 monazite grains were observed as small, anhedral grains ranging from 2-50µm. Monazites were observed in samples from all orebodies investigated and monazites were present in 55% of samples. Samples do not indicate consistent distribution throughout the copper orebodies (Full descriptions of individual samples in Appendix E). All monazites observed have minimal inclusions and appear to have an association with chalcopyrite and pyrite 1 in the copper system (Figure 11). Monazite grains from the 500 orebody are ~ 25µm and are more euhedral compared to monazites observed from the 650 orebody. Monazite from the 650 orebody co-exists with chalcopyrite, pyrite 1 and cobaltite as inclusions associated with the previously mentioned atoll structure of pyrite 1 grains. The 650 orebody contained the largest abundance of monazite (N=18, Appendix E). Monazites from the 3000 and 3500 orebodies, were observed in chalcopyrite, silica dolomite in remobilisation veins and a singular grain in galena.



Sample 6086: Monazite (mnz) in chalcopyrite (cpy) with cobaltite (cob) and pyrite 1 (py) atoll structures adjacent



Sample 6055: Monazite (mnz) in chalcopyrite (cpy)

Sample 6080: Blebby monazite (mnz) in silica dolomite with chalcopyrite (cpy) and pyrite 2 (py)

Figure 11: BSE images of monazites located in the following mine locations (a) & (b) 28B N67 NEXC, 3000-3500 orebodies, (c) & (d) V30 East Decline. 11/L 1361, 650 orebody, (e) 500 copper orebody, lode material, (f) V30 vertical. 11/L 423, 650 orebody

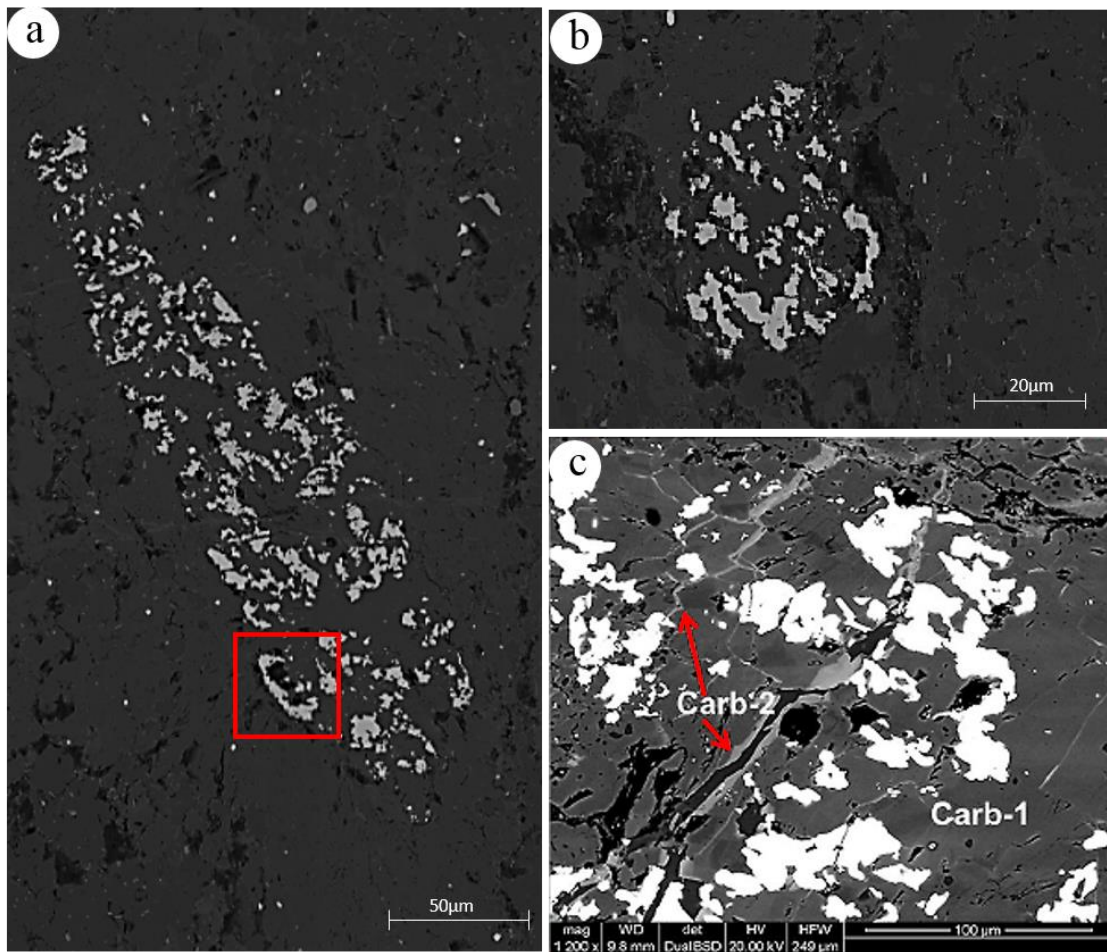


Figure 12: individual BSE images of (a) monazite A and (b) monazite B and (c) detailed inset of carbonate breakup of monazite A

4.3.2 U-PB MONAZITE GEOCHRONOLOGY

Monazite grains identified through SEM EDS observations were initially considered for geochronology analyses. However, the small size of the monazites meant they were unable to be analysed by U-Pb geochronology laser analyses. In situ U-Pb dating of potential hydrothermal monazite was undertaken on a large fractured monazite identified in a previously collected sample from the 1100 orebody (19CQ356DDR012, see Taylor, 2016) (Figure 12). This sample is composed of brecciated siliceous shale, with coarse carbonate-silica infill, as well as coarse grained euhedral pyrite (pyrite 2) and trace amounts of chalcopyrite. The irregular shape of the fractured monazites made

spot analyses placement challenging. Two monazites (hereinafter known as monazite A and monazite B) were present as ~40-250 micron inclusions in siliceous shale (Figure 12a, c). The broken grains may represent a larger grain brecciated by later hydrothermal fluids. Both monazite grains are brecciated by the two Mount Isa pre-ore carbonate events (carbonate 1 and carbonate 2).

A total of 32 analyses were undertaken with 9 excluded because of the poor analyses recorded or discordant ($\pm 10\%$). 23 concordant analyses of in-situ hydrothermal monazites in sample 19CQ356DDR012 yielded a weighted average $^{207}\text{U}/^{206}\text{Pb}$ age of $1614 \pm 52\text{Ma}$. Monazite A had a weighted average of $1638 \pm 95\text{Ma}$ and monazite B had a weighted average of $1535 \pm 61\text{Ma}$ (Figure 14a and b). There was large variation in the individual error ages of the two monazite grains analysed ($\pm 95\text{Ma}$ and $\pm 61\text{Ma}$). When discordant data was removed age uncertainties increased significantly because of the relatively low number of analyses collected (Figure 12).

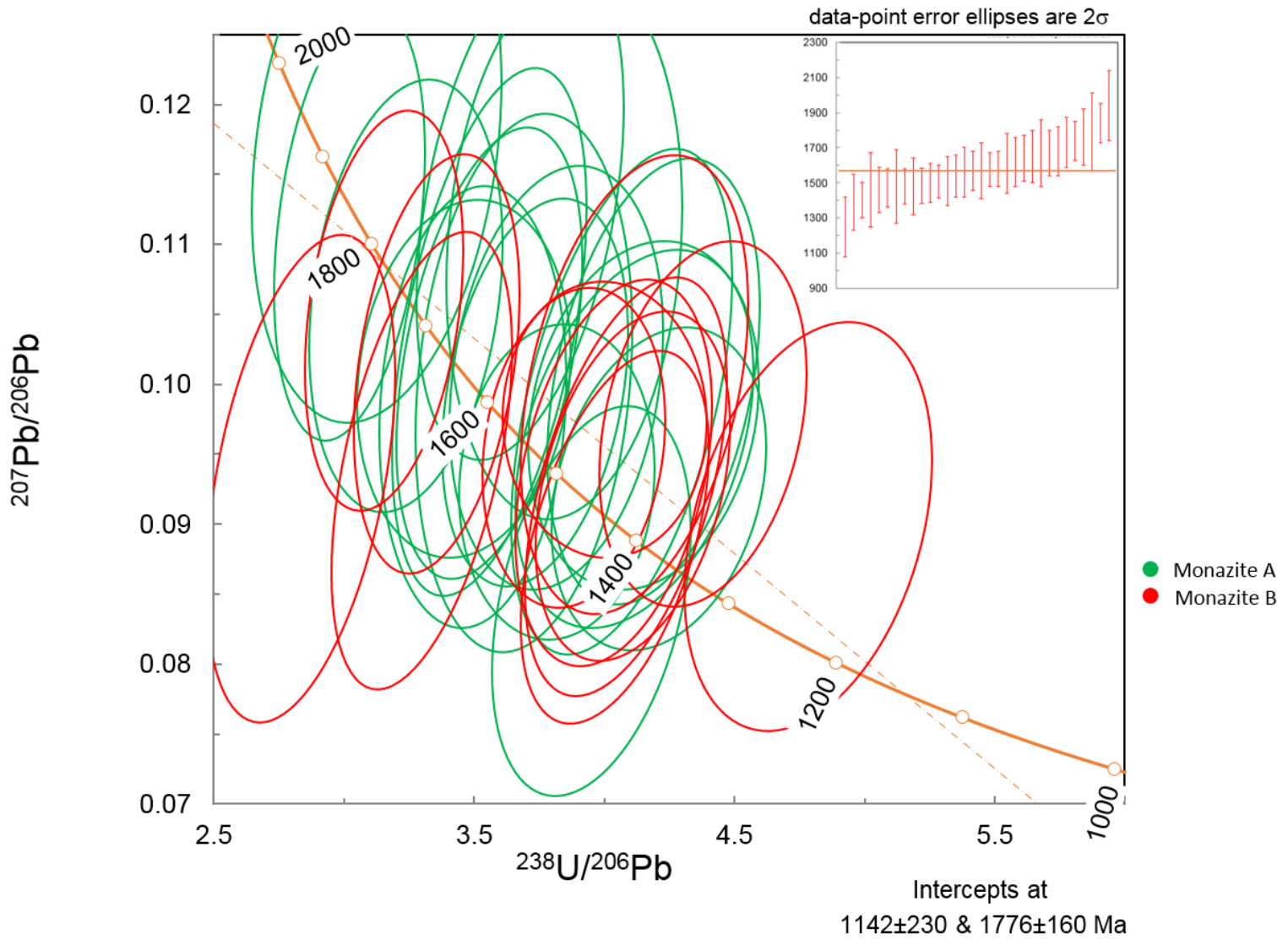


Figure 13: U-Pb Terra-Wasserberg Concordia plot of monazite data with both analyses from sample 19CQ356DDR012

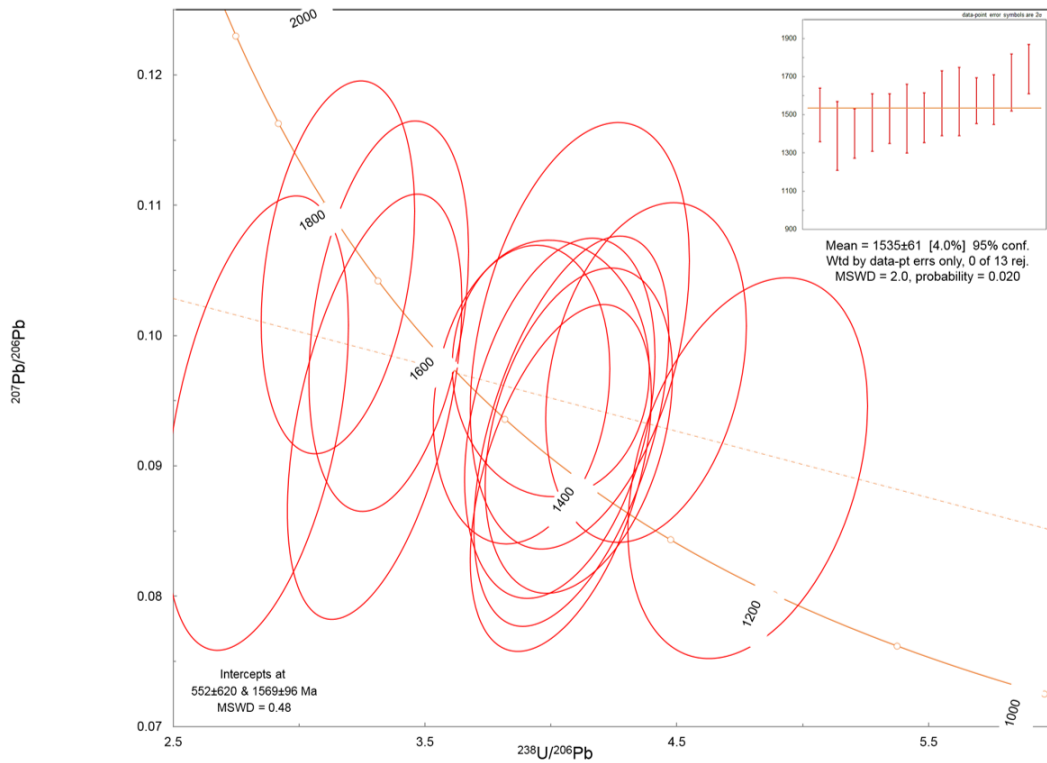
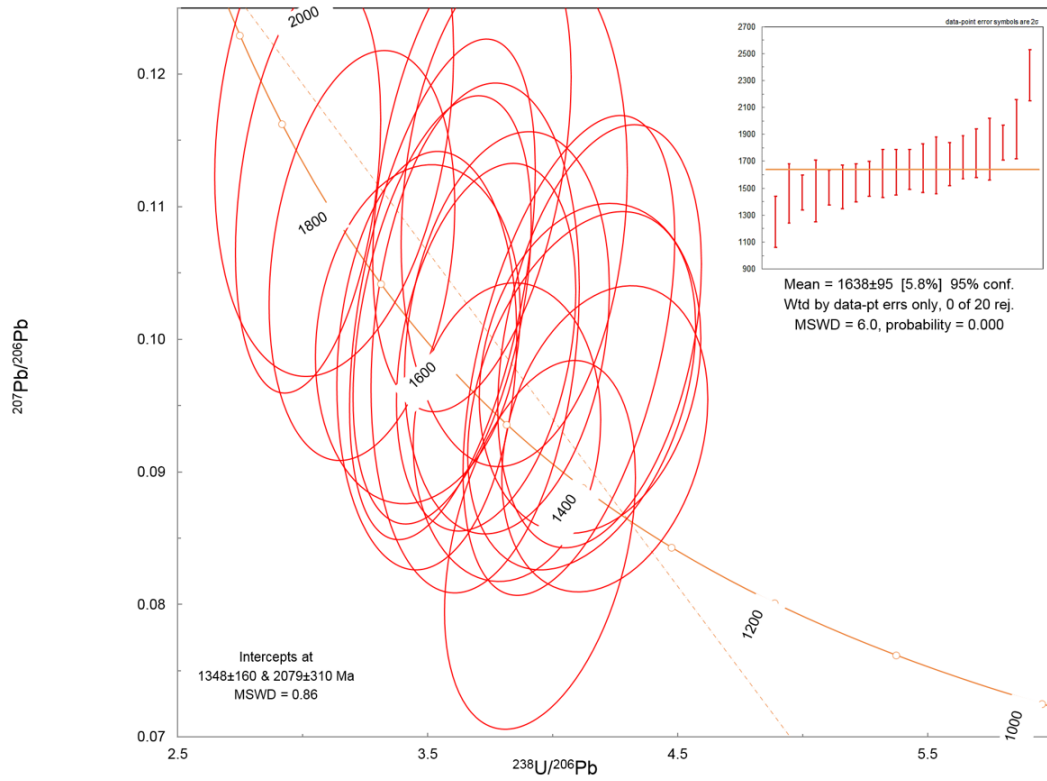


Figure 14: Pb loss trend of monazite analyses (a); uncorrected $^{207}\text{U}/^{206}\text{Pb}$ weighted mean age of analyses from sample 19CQ356DDR012 (b) monazite 1 and (c) monazite 2

5. DISCUSSION

5.1 Cobalt

Cobaltite is a sulphosalt mineral which has been identified within the Mount Isa copper orebodies for an extended period of time (Blanchard and Hall 1942; Croxford, 1974; Mathias and Clark 1975), however, has not been the focus of detailed mineralogical or geochemical studies. Cobaltite is structurally similar to pyrite (FeS_2), with the replacement of a sulphur atom with an arsenic atom. This structural similarity may be a factor as to why cobaltite is found in atoll structures with framboidal pyrite 1.

Encompassing of fine grained pyrite (pyrite 1) atoll structures by cobaltite indicates cobaltite post-dates formation of pyrite 1. This is consistent with work completed by Duckworth and Santaguida (2007) and Taylor (2016). Economic sulphide minerals including cobaltite were deposited in the same hydrothermal sequence, deposited after pyrite 1. Cobaltite is abundant in the 500, 650, 3000, and 3500 orebodies (Figure 3, Duckworth and Santaguida 2007). Co located from the 3500 orebody has a higher Co concentration (33.6% Co) to that in the 1100 orebody (31.82% Co) (Croxford 1974). This supports Hinde's (1994) hypothesis that the deeper orebodies (3000/3500) contain a higher abundance of Co. It is postulated that deeper orebodies in the Mount Isa copper deposit have a higher Co concentration due to the larger proportion of siliceous alteration rock types (Perkins, 1984).

Willyamite was originally discovered at Consols mine, Broken Hill, NSW (Pittman, 1893) and is defined as the portion of the $(\text{Co}, \text{Ni})\text{SbS}$ series with an abundance of Co (Cabri et al, 1970). It has also been identified more recently at the Hultebo Pb-Zn deposit in Sweden (Dobbe, 1991) and the Outokumpu Cu-Zn mine in Finland (Weiser,

2008). The identification of ullmannite and willyamite at Mount Isa is the first occurrence recorded of these minerals outside of Broken Hill in Australia. Willyamite forms a solid solution series with ullmannite and cobaltian ullmannite with ullmannite and cobaltian ullmannite crystallising above 550°C (Bayliss, 1969). The presence of cobalt-bearing minerals and their subsequent paragenesis with chalcopyrite and pyrite indicate variability with the main mineralisation stage. Cobaltite has an estimated formation temperature of 300-350°C (Munro-Smith, 2006) while chalcopyrite temperature is estimated at 225°C (O'Meara, 1961). The variations in temperature are indicative of a prolonged mineralisation sequence or multiple mineralising events. This supports work by Perkins (1997), which implies that chalcopyrite was the youngest sulphide deposited in the main economic mineralisation stage.

Through the data presented in this study, it can be concluded that cobaltite is the dominant Co-bearing mineral in the Mount Isa copper system. However, systematic sampling of additional orebodies could help further define the distribution of Co. Based on the results obtained in this study, chalcopyrite contains greater amounts of Co compared to that of pyrite, which is contradictory to petrological observations of cobaltite commonly associated with pyrite 1. Croxford (1975) identified that cobaltite is generally absent from in the copper ore with the exception of where chalcopyrite veins intersect pyrite. This indicates that there may be a possible hydrothermal influence on pyrite 1 from the later stage chalcopyrite which resulted in the precipitation of Co-rich cobaltite from the hydrothermal fluid.

5.2 Silver

Tetrahedrite and boulangerite are part of the sulphosalts mineral group, which commonly exhibit element substitution within their crystal lattice and co-exist or are inclusions in other minerals in economic orebodies (Hall, 1971). ICP-MS analyses indicate that tetrahedrite and boulangerite were non-stoichiometric (Appendix 3) a common characteristic of tetrahedrite that rarely presents as the ideal chemical formula $(\text{Cu,Fe})_{12}\text{Sb}_4\text{S}_{13}$ (Riley, 1974).

Riley (1974) identified tetrahedrite-freibergite series minerals in the Pb-Zn-Ag system at Mount Isa. Observations of freibergite within galena and grain contacts with chalcopyrite, pyrite and gangue are consistent with the results of this study. Results obtained from this study indicate that samples were argentian tetrahedrite rather than freibergite, as no LA-ICP MS analyses contained Ag content exceeding 20%. Based on petrological and textural observations from this study, it is proposed that cobaltite, chalcopyrite, galena, tetrahedrite and boulangerite precipitated from the same prolonged hydrothermal fluid stage.

Assay data from Ag-Pb rich samples collected from 28B N67 NEXC (Appendix D) support the relationship between galena and tetrahedrite. No clear relationship between the location of acanthite and sternbergite and their abundance was found, however, both were observed in contact with chalcopyrite, indicating they may have precipitated before chalcopyrite.

Trace elements commonly occurring as inclusions in chalcopyrite include, Pb, Bi, Zn and Ba, while elements which substitute stoichiometrically into the crystal lattice comprise of Ag (for Cu), In, Sn and Zn (for Fe), and Se (for S) (Huston, 1995).

Argentiferous chalcopyrite $((\text{Cu,Ag})\text{FeS}_2)$ has been previously identified at Hilton Pb-

Zn mine near Mount Isa Mines, with all chalcopyrite within the Pb-Zn system containing Ag in solid solution regardless of mineralisation style and location (Knights, 1985). Ag levels in chalcopyrite vary significantly which is consistent to Ag content in chalcopyrite from Hilton mine (Harris et al, 1984). Although most Ag in chalcopyrite occurs as substitutions for Cu in the lattice (eg. Harris et al 1984), high values associated with high Pb levels may result from inclusions of argentiferous galena. Based on the lack of galena present where chalcopyrite analyses were taken, it is unlikely this is the case for the Mount Isa Cu deposit. This indicates that Ag occurrence in chalcopyrite in the Mount Isa copper system is due to solid solution Ag substitution for Cu in the crystal lattice. Chalcopyrite is a poor trace element carrier compared to galena and sphalerite (George et al 2016) indicating that the abundance of Ag in chalcopyrite may be attributed to the absence of other base metal sulphides.

Based on the results from this study, the Ag mineralogy of the Mount Isa copper deposit is heterogeneous and sparsely distributed through the system. The majority of Ag can be found in tetrahedrite as a mineral inclusion in galena. Therefore, areas of the mine containing a high abundance of galena are more likely to contain profitable amounts of Ag. The distribution of argentiferous chalcopyrite within the copper orebodies is undetermined at this point in time as only samples from the 3500 orebody were ablated (CLL-02 and CLL-03).

5.3 Monazite

Based on textural descriptions of hydrothermal monazite in Schandl & Gorton (2004) and petrological observations from this study, the monazites investigated in sample 19CQ356DDR012 are proposed to be hydrothermal in origin. Because of a relatively large error in the age ($1614 \pm \pm 52$ Ma) produced from the monazite, several important

dates within the Mount Isa inlier correlate with the age obtained through U-Pb geochronology. These events include the formation of the Urquhart shale formation at Mount Isa (1652 ± 7 Ma), formation of Urquhart shale at George Fisher (1655 ± 4 Ma) (Page, 2000). It also correlates strongly with D₁ date of 1610 ± 13 while D₂ (1544 ± 12) and D₃ (1510 ± 13) (Page and Bell 1986), dates do not relate to the combined monazite date.

Based on petrographic observations, it is proposed monazites dated were placed before the two carbonate events in the Mount Isa copper deposit paragenesis. Monazite appears to have a strong association with chalcopyrite, which is part of a later paragenetic sequence (Table 1). The dates obtained by analysis are consistent with the interpretation that the monazite may have originated syngenetically with the pyrite 1 stage of paragenesis. However, when the monazite grains are individually analysed, Monazite B correlates (1535 ± 61 Ma) with the main mineralisation stage 1523Ma (Perkins 1999). This implies that localised fluid may have caused heterogeneous resetting of monazite ages during fluid-related alteration (William et al, 2011) during the economic sulphide stage. Cu mineralisation at Mount Isa is determined to be circa 1523 Ma (Perkins, 1999) therefore indicating monazite sampled may not have come in the same stage or was reset by economic sulphide mineralisation. It is proposed by this study that monazite was either (a) syngenetically deposited with pyrite 1, which was partially reset by the main copper ore fluids during D₁ or (b) were part of a discrete hydrothermal fluid stage around the time of pyrite 1 deposition which has not been previously identified. Petrological data are consistent with the interpretation that monazite was introduced into the Mount Isa system at the same time as chlorite±quartz±pyrite-1.

Because of the limited number of laser analyses, there is a large error range for both concordant and discordant analyses; when only concordant data is selected, the error range increases significantly. As a result of this large error, it is hard to constrain an age which correlates with the monazites in the system.

Implications on ore genesis

The heterogeneous variation of the trace metals Ag and Co is consistent with a hydrothermal fluid source with variable composition (Williams, 1998). The distribution of minor metals Ag and Co in the Cu and Zn-Pb systems is paragenetically similar indicating they may have formed co-genetically. All minerals identified in this study, with the exception of boulangierite, have been previously identified in the Zn-Pb deposit. The deposit Co and Ag variation is consistent with the presently accepted paragenesis and is indicative of a concurrent Cu, Pb and Zn mineralising system during prolonged sulphur enriched hydrothermal events. Observations and interpretations are consistent with work done by Taylor and Lilly (2016), indicating there is only one stage of ore-related sulphidation in the Mount Isa Cu-Pb-Zn-Ag system.

Mining challenges and economic significance

Because of cobaltite's association with pyrite, it is estimated that ~10,000 tpa of Co is discarded in the mine tailings at Mount Isa Mines (Geological survey of Queensland, 2014). The price of Co has almost doubled since 2013 as it is used in renewable energy in rechargeable battery electrodes and in superalloys, If the Co were able to be extracted from current tailings, it could be worth ~\$760 million AUD per annum, based on average Co price of \$26.76 USD/lb as of September 2017. The main challenge for removing Co

from tailings is separating the cobaltite from pyrite. A patent for the process for the selective dissolution of Co from cobaltite-pyrite concentrates was invented by Stanley et al (1982). The problem with this is it would require the hydrometallurgical process to be performed after waste material has already been sent to the tails. An alternative method which is being studied, is the use of thermophilic bioleaching technology to extract Co from tailings. Co is extracted into cobalt oxalate using leaching bacteria *Acidithiobacillus ferrooxidans*, *Acidithiobacillus thiooxidans*, and *Leptospirillum ferrooxidans*. A study by Chen et al (2016) obtained a recovery rate for Co of more than 95% using this technique. Bacterial oxidation is considered a more environmentally friendly method of metal extraction and reduces the risk of acid leach draining from pyrite in tailings.

6. CONCLUSIONS

- Observed Co is hosted by the minerals cobaltite and willyamite (hypothesis 1).
- Observed cobaltite post-dates the deposition of pyrite 1 (fine grained pyrite) and paragenetically pre-dates the deposition of economic sulphides during the extended paragenetic Stage 4.
- Ag mineral paragenesis consists of argentian tetrahedrite, acanthite, sternbergite and in solid-solution within chalcopyrite and galena (hypothesis 2).
- Chalcopyrite analysed by this study can contain up to 3.9% Ag, with an average of 182.2ppm.
- Ag in the Mount Isa copper orebodies demonstrates the same paragenesis and mineral relationships to that of the Mount Isa Pb-Zn-Ag orebodies.
- Findings of this study are consistent with the ore genesis model of Taylor and Lilly (2016).

- Co appears to have a higher concentration within the 3000/3500 orebodies compared to the 500/650 orebodies.
- Different orebodies have different abundances of different trace minerals, consistent with a prolonged and complex hydrothermal system (hypothesis 3).
- Trace minerals (including Co, Ag and monazite) are irregularly distributed throughout the Mount Isa copper orebodies (hypothesis 3).
- Hydrothermal monazites A and B sampled yielded a combined weighted average $^{207}\text{U}/^{206}\text{Pb}$ age of 1614 ± 52 Ma.
- The calculated monazite age is chronologically between the accepted ages for deposition of the Urquhart Shales ($1654 \text{ Ma} \pm 4 \text{ Ma}$) and the accepted age for copper mineralisation associated with the Isan Orogeny (1590-1500 Ma).

7. RECOMMENDATIONS FOR FURTHER STUDY

Based on the large error bars in this study, it is recommended that further studies are conducted on additional monazites from the Mount Isa system to better constrain the age and subsequent error bars of monazite in the Mount Isa system to further constrain paragenesis. Additionally, the use of alternative dating techniques such as rutile dating may be beneficial in determining whether mineralisation occurred in a single event and to narrow down the error bars associated with U-Pb geochronology. Further research is also recommended for geochemical analyses of the Co-bearing mineral willyamite to help understand additional trace metals Co and Ni within the deposit and their association with Sb. Finally, representative assaying of chalcopyrite from the orebodies to see if argentiferous chalcopyrite is consistently found throughout the Cu system would

be beneficial in determining where silver is located in the system and whether it is consistent with observations from the Zn-Pb system.

8. ACKNOWLEDGEMENTS

I would like to acknowledge the many people and organisations who have assisted me with this research. Firstly, I would like to thank my supervisor Dr Richard for all his support and encouragement this year. I would also like to thank Mount Isa Copper Operations (MICO) for assisting me in my field work and sample collection and for supporting my project this year. Special thanks to Dan Taylor and the graduate geologists at MICO for being so enthusiastic and helpful during my time at Mount Isa. I would like to thank the Playford trust scholarship program and Scantech for providing me with my scholarship which financially assisted me this year. The staff at Adelaide Microscopy, in particular David Kelsey and Sarah Gilbert who gave expert advice throughout my time there. To the 2017 honours cohort which made long hours at university bearable and at times fun. In particular my fellow honours students which were part of the A.W.E.S.O.M.E.S research unit, who were amazing at providing support and encouragement throughout the year.

9. REFERENCES

- BAYLISS, P. (1969). X-ray data, optical anisotropism, and thermal stability of cobaltite, gersdorffite, and ullmannite. *Mineralogical Magazine*, 37(285), 26-33.
- BELL, T., PERKINS, W., & SWAGER, C. (1988). Structural controls on development and localization of syntectonic copper mineralization at Mount Isa, Queensland. *Economic Geology*, 83(1), 69-85.
- BETTS, P., & LISTER, G. (2002). Geodynamically indicated targeting strategy for shale-hosted massive sulfide Pb-Zn-Ag mineralisation in the Western Fold Belt, Mt Isa terrane. *Australian Journal of Earth Sciences*, 49(6), 985-1010.
- BLANCHARD, R., & HALL, G. (1942). *Rock deformation and mineralization at Mount Isa*.
- BRILL, B. (1989). Trace-element contents and partitioning of elements in ore minerals from the CSA Cu-Pb-Zn deposit, Australia, and implications for ore genesis. *The Canadian Mineralogist*, 27(2), 263-274.
- CABRI, L., HARRIS, D., STEWART, J., & ROWLAND, J. (1970). Willyamite redefined. *Aust. Inst. Min. Metall. Proc.* 233, 95-100.
- CARTER, S. (1953). *Mount Isa Mines*. Paper presented at the Geology of Australian Ore Bodies. Fifth Empire Mining and Metallurgical Congress Australia and New Zealand.
- CHEN, G., YANG, H., LI, H., & TONG, L. (2016). Recovery of Cobalt as Cobalt Oxalate from Cobalt Tailings Using Moderately Thermophilic Bioleaching Technology and Selective Sequential Extraction. *Minerals*, 6(3), 67.
- CONAGHAN, E., HANNAN, K., & TOLMAN, J. (2003). Mount Isa Cu and Pb-Zn-Ag deposits, NW Queensland, Australia. *A compilation of geochemical case histories and conceptual models. CRC LEME, Canberra, Australia*, 1-3.
- CROXFORD, N. (1974). Cobalt mineralization at Mount Isa, Queensland, Australia, with references to Mount Cobalt. *Mineralium Deposita*, 9(2), 105-115.
- DAVIS, T. (2004). Mine-scale structural controls on the Mount Isa Zn-Pb-Ag and Cu orebodies. *Economic Geology*, 99(3), 543-559.
- DOBBE, R. (1991). Ullmannite, cobaltian ullmannite and willyamite from Tunaberg, Bergslagen, central Sweden. *The Canadian Mineralogist*, 29(2), 199-205.


- DUCKWORTH, R., & SANTAGUIDA, F. (2007). Trace metal distribution within the copper mineralization zones at the Mount Isa Mine: ERGU James Cook University.
- FISHER, N. (1960). *Review of evidence of genesis of Mt. Isa*. Paper presented at the Isa orebodies: Rept. 21st Int. Geol. Congress, Copenhagen, Part.
- GRONDIJS, H., & SCHOUTEN, C. (1937). A study of the Mount Isa ores [Queensland, Australia]. *Economic Geology*, 32(4), 407-450.
- GULSON, B., PERKINS, W., & MIZON, K. (1983). Lead isotope studies bearing on the genesis of copper orebodies at Mount Isa, Queensland. *Economic Geology*, 78(7), 1466-1504.
- HALL, A. (1971). *The mineralogy of some synthetic sulphosalts*. Durham University.
- HARRIS, D., CABRI, L., & NOBILING, R. (1984). Silver-bearing chalcopyrite, a principal source of silver in the Izok Lake massive-sulfide deposit; confirmation by electron-and proton-microprobe analyses. *The Canadian Mineralogist*, 22(3), 493-498.
- HEAD, K. (2007). MICO 3000 & 3500 orebody characterisation project: Sulphides.
- HINDE, J. (1994). *A Summary of the Geology and Genesis of the Mount Isa Copper Orebodies*.
- HUSTON, D., SIE, S., SUTER, G., COOKE, D., & BOTH, R. (1995). Trace elements in sulfide minerals from eastern Australian volcanic-hosted massive sulfide deposits; Part I, Proton microprobe analyses of pyrite, chalcopyrite, and sphalerite, and Part II, Selenium levels in pyrite; comparison with delta 34 S values and implications for the source of sulfur in volcanogenic hydrothermal systems. *Economic Geology*, 90(5), 1167-1196.
- KNIGHT, C. (1957). Ore genesis; the source bed concept. *Economic Geology*, 52(7), 808-817.
- KOŁODZIEJCZYK, J., PRSEK, J., ASLLANI, B., & MALIQI, F. (2016). The paragenesis of silver minerals in the Pb-Zn Stan Terg deposit, Kosovo: an example of precious metal epithermal mineralization. *Geology, Geophysics and Environment*, 42(1).
- LILLY, R. (2017). *Mount Isa Cu-Pb-Zn deposit including George Fisher deposit*.
- LONG, R. (2010). *The Paroo Fault and the Mount Isa copper orebodies; a revised structural and evolutionary model, Mt Isa, Queensland, Australia*. James Cook University.
- LUDWIG, K. (2003). *User's manual for Isoplot 3.00: a geochronological toolkit for Microsoft Excel*: Kenneth R. Ludwig.
- MATHIAS, B., & CLARK, G. (1975). Mount Isa copper and silver-lead-zinc orebodies—Isa and Hilton mines. *Economic Geology of Australia and Papua New Guinea*, 1, 351-372.
- MCGOLDRICK, P. (1986). *Volatile and Precious Metal Geochemistry of the Mount Isa Ores and their Host Rocks*. University of Melbourne.
- MILLER, B. (2006). Characterisation and timing of faults with respect to copper mineralisation and talc alteration in the Northern 3500 orebody, Mount Isa, Northwest Queensland.
- MUNRO-SMITH, V. (2006). Cobalt mineralisation in selected Australian deposits.
- MURRAY, W. (1961). Notes on Mount Isa geology: Proceedings of the Australasian Institute of Mining and Metallurgy, v. 197.
- NEUDERT, M. (1983). *A depositional model for the upper Mount Isa group and implications for ore formation*. (PhD), Australian National University
- O'MEARA, A. (1961). *Contribution to the study of the Mount Isa copper orebodies*. Paper presented at the Proceedings of the Australasian Institute of Mining and Metallurgy.
- PAGE, R., JACKSON, M., & KRASSAY, A. (2000). Constraining sequence stratigraphy in north Australian basins: SHRIMP U–Pb zircon geochronology between Mt Isa and McArthur River. *Australian Journal of Earth Sciences*, 47(3), 431-459.
- PAINTER, M. (2003). The geochemical and mineralogical haloes around the Mt Isa base metal orebodies.
- PATON, C., HELLSTROM, J., PAUL, B., WOODHEAD, J., & HERGT, J. (2011). Iolite: Freeware for the visualisation and processing of mass spectrometric data. *Journal of Analytical Atomic Spectrometry*, 26(12), 2508-2518.
- PERKINS, C., HEINRICH, C., & WYBORN, L. (1999). 40 Ar/39 Ar geochronology of copper mineralization and regional alteration, Mount Isa, Australia. *Economic Geology*, 94(1), 23-36.
- PERKINS, W. (1984). Mount Isa silica dolomite and copper orebodies; the result of a syntectonic hydrothermal alteration system. *Economic Geology*, 79(4), 601-637.
- PERKINS, W. (1990). Mount Isa copper orebodies. *Geology of the mineral deposits of Australia and Papua New Guinea: Australasian Institute of Mining and Metallurgy, Monograph*, 14, 935-941.
- PERKINS, W. (1997). Mount Isa lead-zinc orebodies: Replacement lodes in a zoned syndeformational copper-lead-zinc system? *Ore Geology Reviews*, 12(2), 61-110.



- PITTMAN, E. (1893). Note on the occurrence of a new mineral at Broken Hill. *Proc. Royal Soc. NSW*, 27, 365-375.
- PRIDMORE, D., & SHUEY, R. (1976). The electrical resistivity of galena, pyrite, and chalcopyrite. *American Mineralogist*, 61(3-4), 248-259.
- RAYNOR, E. (1953). *Cobalt mineralization in the Cloncurry district*. Paper presented at the Geology of Australian Ore Deposits. (5th Empire Mining and Metallurgical Congress: Melbourne).
- RILEY, J. (1974). The tetrahedrite-freibergite series, with reference to the Mount Isa Pb-Zn-Ag orebody. *Mineralium Deposita*, 9(2), 117-124.
- SCHANDL, E., & GORTON, M. (2004). A textural and geochemical guide to the identification of hydrothermal monazite: criteria for selection of samples for dating epigenetic hydrothermal ore deposits. *Economic Geology*, 99(5), 1027-1035.
- SCHOUTEN, C. (1946). The role of sulphur bacteria in the formation of the so-called sedimentary copper ores and pyritic ore bodies. *Economic Geology*, 41(5), 517-538.
- STILLWELL, F., & EDWARDS, A. (1945). The mineral composition of the Black Star copper ore body, Mount Isa, Queensland. *Proc. Australasian Inst. Min. Metall*(139), 149-159.
- SWAGER, C. (1985). Syndeformational carbonate-replacement model for the copper mineralization at Mount Isa, Northwest Queensland; a microstructural study. *Economic Geology*, 80(1), 107-125.
- TAYLOR, R. L., R. (2016). *Is Mount Isa a zoned carbonate replacement system?*
- WEISER, T., KOJONEN, K., & LODZIAK, J. (2008). New data of eskolaite, Zn-bearing chromite, willyamite and ullmannite from the Outokumpu mine, eastern Finland. *BULLETIN-GEOLOGICAL SOCIETY OF FINLAND*, 80(1), 5.
- WILDE, A. (2011). Mount Isa copper orebodies: improving predictive discovery. *Australian Journal of Earth Sciences*, 58(8), 937-951.
- WILDE, A., JONES, P., GESSNER, K., AILLERES, L., GREGORY, M., & DUNCAN, R. (2006). A geochemical process model for the Mount Isa copper orebodies. *Economic Geology*, 101(8), 1547-1567.
- WILLIAMS, M., JERCINOVIC, M., HARLOV, D., BUDZYŃ, B., & HETHERINGTON, C. (2011). Resetting monazite ages during fluid-related alteration. *Chemical Geology*, 283(3), 218-225.
- WILLIAMS, P. (1998). An introduction to the metallogeny of the McArthur River-Mount Isa-Cloncurry minerals province. *Economic Geology*, 93(8), 1120-1131.



APPENDIX A: LASER PARAMETERS USED AT ADELAIDE MICROSCOPY ON LA-ICP-MS



<i>LA-ICP-MS</i>		
	Sulphides	Monazite
<i>Brand and model</i>	<i>Agilent 7700x ICP-MS</i>	<i>Agilent 7900x ICP-MS</i>
<i>Forward power</i>	<i>1350W</i>	<i>1350W</i>
<i>Cool (Ar)</i>	<i>15</i>	<i>15</i>
<i>Auxiliary (Ar)</i>	<i>0.89</i>	<i>0.89</i>
<i>Carrier (He)</i>	<i>0.35</i>	<i>0.35</i>
<i>Sample (Ar)</i>	<i>1.06</i>	<i>1.06</i>
<i>Laser</i>		
<i>Type of laser</i>	<i>ArF Excimer</i>	<i>ArF Excimer</i>
<i>Brand and model</i>	<i>Resolution LR (Resonectice)</i>	<i>New Wave UP-213 laser system</i>
<i>Laser wavelength</i>	<i>213nm</i>	<i>213nm</i>
<i>Pulse duration</i>	<i>10-40s (variable depending on grain size)</i>	<i>20ns</i>
<i>Spot Size</i>	<i>15-70µm</i>	<i>7 µm</i>
<i>Laser Energy</i>	<i>40 mJ</i>	<i>75mJ</i>
<i>Repetition rate</i>	<i>5Hz</i>	<i>10Hz</i>
<i>Energy attenuation</i>	<i>27%</i>	<i>100%</i>
<i>Laser Fluence</i>	<i>~4 J/cm-2</i>	<i>~9.5 ~J/cm-2</i>
<i>Laser warm up (background collection)</i>	<i>30s</i>	<i>30s</i>
Data Acquisition Parameters		
<i>Data acquisition protocol</i>	<i>Time-resolved analysis</i>	<i>Time-resolved analysis</i>
<i>Cleaning method</i>	<i>Firing 5 pulses followed by washout</i>	<i>Firing 5 pulses followed by washout</i>
<i>Detection mode</i>	<i>Pulse counting</i>	<i>Pulse counting</i>
<i>Detector Deadtime</i>	<i>3.68ns</i>	<i>3.68ns</i>
<i>Background collection</i>	<i>30s</i>	<i>30s</i>
<i>Ablation Time</i>	<i>30s (variable depending on grain size)</i>	<i>30s</i>
<i>Ablation Sequence</i>	<i>2 x Mass-1, 2 x GSD, 20 x Unknown</i>	<i>2 x MAdel, 2 x 222, 2 x Ambat, 15 x Unknown</i>
Standardisation and Data Reduction		
<i>Primary standard</i>	<i>MASS-1</i>	<i>MAdel</i>
<i>Secondary standard</i>	<i>GSD</i>	<i>222, Ambat</i>
<i>Data reduction software</i>	<i>In House Excel</i>	<i>In House Excel</i>


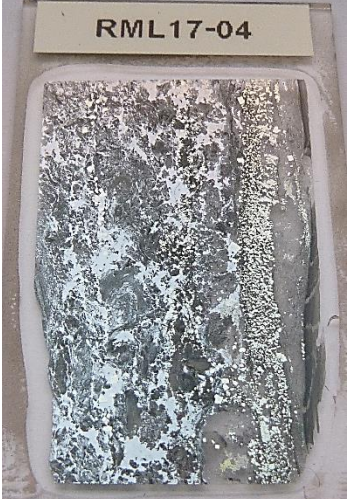
APPENDIX B: FULL PETROLOGY ANALYSIS OF ALL 20 SAMPLES



Sample	Orebody	Description	Image
Thesis sample 01 (CLL-01)	3500	This sample is dominated by chalcopyrite, with sub-rounded coarse grained pyrite and small amounts of pyrrhotite. In the bottom right hand side of the section is significant sulphide veining with triangular infill textures.	



<p>Thesis sample 02 (CLL-02)</p>	<p>3500</p>	<p>Major sulphides present are chalcopyrite and pyrite, with minor galena and pyrrhotite present. Main gangue mineral in this sample is quartz. There is high texture variation of sulphides within the sample, ranging from massive, blebby and cubic structures.</p>	
<p>Thesis sample 03 (CLL-03)</p>	<p>3500</p>	<p>This sample appears to have a higher cpy content compared to previous samples. There is also a higher percentage of gangue minerals, possibly buck quartz. Chalcopyrite appears to have been part of a later mineralisation stage as there are strong infill textures present. In the bottom left hand side of the sample is a highly reflective grain which was determined to contain willyamite, galena and native bismuth. Cobaltite present in large grains, appears to have a relationship with pyrite, forming in a later mineralisation phase, causing many of the “cubic” cobaltite grains to have a pyrite “core” within major sulphides within the sample.</p>	



Thesis sample 04 (CLL-04)	3200	<p>The sample consists mainly of chalcopyrite with some gangue mineral present (quartz?) Large amount of chalcopyrite indicates high copper content. Appears to have a left-right directional movement (possibly from when thin section was cut). Veining present, cutting through the sulphide mineralisation. Possible pyrrhotite present but had to separate from chalcopyrite (possibly different version of cpy?) Pyrite appears to be absent from this sample.</p>	
Thesis sample 05 (CLL-05)	3200	<p>The sample is largely dominated by chalcopyrite with areas of pyrrhotite in areas but hard to distinguish with naked eye. Appears to be very fine infill texture of gangue mineral, but possibly points of imperfection within the thin section. Small traces of pyrite present themselves as rounded nodules. In some areas, gangue minerals have a vesicular texture which overprints previous mineralisation.</p>	



<p>Thesis sample 06 (RML 17-01)</p>	<p>28B N67 NEXC</p>	<p>This sample contains large quantities of chalcopyrite and pyrrhotite, with coarse grained pyrite and what is believed to be galena in trace amounts. Other possible minerals include tetrahedrite and willyamite. The blue mineral mainly appears around cpy in this particular sample. Pyrite is coarse grained, cubic or nodular in appearance and appears to have been remobilised. Some grains of pyrrhotite appear to have a variation in colour, which is a possible indicator of argentopyrite.</p>	
<p>Thesis sample 07 (RML 17-02)</p>	<p>28B N67 NEXC</p>	<p>Galena and pyrrhotite present as the dominant minerals in this sample, with a small percentage of chalcopyrite. Sphalerite is also present, within the galena mineralisation. The galena in this sample has a “teeth texture” which is assumed to be a late stage mineralisation infill texture. RML 17-02 contains two colour variations in galena, one which is determined to be sphalerite and the other which is potentially tetrahedrite. This variation is consistent throughout the main galena vein of the sample. Coarse grained pyrite is in the sample, appearing with a cubic crystal structure and ranging from 20-50um grain size.</p>	



<p>Thesis sample 08 (RML 17-03)</p>	<p>28B N67 NEXC</p>	<p>The main sulphides in this sample are galena and pyrrhotite, with pyrrhotite being the bulk and galena evenly distributed. Within the galena mineralisation is two colour variations which is indicative of other minerals. Potential minerals include: galena, tetrahedrite or sphalerite. These “variations” in minerals consistently appear with one another and do not present in any other</p>	 <p>RML17-03</p>
<p>Thesis sample 09 (RML 17-04)</p>	<p>28B N67 NEXC</p>	<p>Galena and pyrite are largely present in the sample as well as both fine and coarse grained pyrite. The fine grained pyrite appears to be localised to the far right hand side of the thin section. Minor pyrrhotite and chalcopyrite are also present. The mineral variation in galena is once again present, to a lesser extent, which appears to be found adjacent to other sulphide grains such as chalcopyrite. What has been determined as sphalerite in previous samples has appeared as blebby grains within galena, however in this sample they appear to be more independent of the galena and more massive grains.</p>	 <p>RML17-04</p>


<p>Thesis sample 10 (RML 17-05)</p>	<p>28B N67 NEXC</p>	<p>Chalcopyrite is depleted in this sample, being only found in trace amounts. On the right hand side of the sample, galena and pyrrhotite intermingle with one another, in an almost interlocking texture. Once again, the variation within the galena appears to be present around chalcopyrite and less frequency when the sample area is dominated by galena alone. This indicates that there may be a possible relationship between chalcopyrite, galena and trace minerals in the orebody. The pyrrhotite has a slight colour variation in areas, which could be indicative of argentopyrite, other possibility is a polishing imperfection. Fine and coarse grained pyrite are found throughout the sample but do not appear to interact with one another.</p>	
<p>Thesis sample 11 (6055)</p>	<p>500</p>	<p>The dominant sulphide in this sample appears to be pyrite with large amounts of chalcopyrite also present. Small traces of galena can be found within the chalcopyrite. Unknown minerals located in pyrite near veining (later determined as tetrahedrite and boulangerite), has not been found in previous sample observations. Pyrite appears to have been altered, as it contains many inclusions/veins. Possible pyrrhotite also present.</p>	

<p>Thesis sample 12 (6079)</p>	<p>Located in V30 vertical. 11/L 64 (V30, vertical 11/L. 64ft 650 copper orebody).</p>	<p>Sulphide minerals present include chalcopyrite, pyrite, pyrrhotite and galena. Possible tetrahedrite/sphalerite present in galena. Bottom section of sample contains angular textures which are indicative of possible zonation.</p>	
<p>Thesis sample 13 (6080)</p>	<p>V30 vertical. 11/L 423.</p>	<p>High abundance of veining in sample, with small trace amounts of cpy in veins. Top section of samples has more interrupted sulphides in comparison to other areas, pyrite appears to be less affected however. Unidentified blue mineral in chalcopyrite, contains inclusion within it and is adjacent to major vein. Possible classification for unknown mineral is tetrahedrite.</p>	

Thesis sample 14 (6084)	V30 East decline. 11/L 80.	Chalcopyrite dominated sample, with some galena present. Unknown trace minerals located as inclusions and imperfections in chalcopyrite. Large amounts of veining present, possible location for further trace minerals.		
Thesis sample 15 (6085)	V30 East Decline. 11/L 809.	Major sulphides present are pyrite, chalcopyrite and pyrrhotite. The majority of sulphide textures appear to be massive/blebby/interrupted. Chalcopyrite contains infill textures. Sample is pyrrhotite rich, coarse grained pyrite appears to be absent. There appears to be an interaction with pyrite, chalcopyrite and pyrrhotite, possible indicator sulphides mineralised in same event?		

<p>Thesis sample 16 (6086)</p>	<p>V30 East Decline. 11/L 1361.</p>	<p>Chalcopyrite and pyrite are mainly nodular in texture, chalcopyrite is dominant sulphide. There also appears to be sulphides within gangue minerals as veining.</p>	
<p>Thesis sample 17 (6110)</p>	<p>T14 East Decline No-2, 11/L. 205.</p>	<p>Two large chalcopyrite samples with pyrite and gangue inclusions. Pyrite is mainly nodular and massive with chalcopyrite associated with it. Pyrrhotite is also present.</p>	

Thesis sample 18 (6111)	T14 East Decline No-2, 11/L. 518.	Sample largely contains buck quartz, with main sulphide present chalcopyrite and chalcopyrite veining. Pyrite is also present in sample. Veining appears to be occurring in chalcopyrite but not in pyrite. <ul style="list-style-type: none">• Gangue veining in cpy on the bottom left hand side of sample	
Thesis sample 19 (6263)	650 copper orebody – Z.74 W. Incline 12 level.	Pyrite and chalcopyrite mottled together, pyrite varies between nodules and disseminated/massive. Bottom left hand side of sample very complicated textures area of interest for SEM. No other major sulphides appear to be present.	

<p>Thesis sample 20 (19CQ356DDR012)</p>	<p>X41 FWL Lens, Level 19C Q356 DDR, reactive ground</p>	<p>Brecciated siliceous shale with coarse carbonate silica, pyrite 2 and minor chalcopyrite</p>	 <p>The photograph shows a rock sample with a light-colored, siliceous matrix. Scattered throughout are dark, angular fragments of pyrite and smaller, more irregular pieces of chalcopyrite. The overall texture is brecciated, with the fragments embedded in a finer-grained material.</p>
--	--	---	--

APPENDIX C: LA-ICP-MS DATA

			¹⁹⁷ Au ppm	¹⁸⁹ Ag ppm	⁶⁵ Cu ppm	⁶⁴ Ni ppm	⁶⁶ Zn ppm	²⁰⁶ Pb ppm	⁵⁹ Co ppm	⁷⁵ As ppm	¹²¹ Sb ppm	²⁰⁹ Bi ppm	¹²⁵ Te ppm
Pyrite	n=7	Mean	0.185	4.91	1780	5.58	4.25	67.6	113	274	21.8	11.5	0.68
		Max	6.5	20.8	14300	10300	151	682	135000	185000	188	38.9	1.4
		Min	0.03	-0.003	5	3.29	3.32	0.37	1.46	16.4	0.039	0.0222	0.45
Chalcopyrite	n=31	Mean	0.94	182.2	323000	690	463	19740	37000	3380	3910	956	0.64
		Max	7600	39000	750000	31400	33100	640000	303000	197800	350000	148000	5500
		Min	0.054	35.8	185000	587	158.8	1.64	0.94	-0.4	2.3	0.939	0.64
Cobaltite	n=46	Mean	0.21	3.3	460	8290	1.24	236	336000	21560000	53	18.2	0.26
		Max	7.5	43.9	58000	19640	46.7	15900	382800	86200000	6390	479	1.76
		Min	-0.005	-0.084	4	1420	-0.65	0.88	184000	10070000	2.82	0.209	-1.2
Tetrahedrite	n=50	Mean	3	115000	195500000	0.049865	30500	785000000	80	16500	325000000	600	2650
		Max	300	4000000	1000000000	270	82000	10000000000	530	89000	1410000000	16300	15000
		Min	-300	0.174	0.82	-300	-10000	35.6	-5	-30000	2.13	-0.0000976	-1500
Boulangerite	n=34	Mean	0.25	340000	515000	0.0209923	8700	55700000	59	19.8	480000	0.9945	1.7
		Max	2900	410000000	490000000	130	9200000	349000000	29000	43000	610000000	16	90000
		Min	-330	6900	26200	-0.27	133	41000	0.43	-100	37000	-0.5	-1700
Galena	n=49	Mean	0.03	409	43	-0.00001	2.7	229000000	0.04	3.2	819	1.85	0.5
		Max	0.4	650000	910000	0.7	18300	280000000	24	34	1180000	2.87	10.9
		Min	-0.24	94	0.3	-0.000056	-1.7	56000000	-0.000202	-6.8	408	0.69	-5

APPENDIX D: SILVER ASSAY DATA

Samples containing Ag mineralogy confirmed by SEM observations (located at 28B N67 NEXC, which links the 3000 and 3500 orebodies) were assayed by ALS minerals with results displayed below. RL grab 3 had up to 696ppm of Ag with 40 percent lead and 0.05% copper.

Sample		Ag	Cu	Pb	Zn	S	Al2O3	As	CaO	Co	Fe	MgO	Sb	SiO2
		ppm	%	%	%	%	%	%	%	%	%	%	%	%
2017RL GRAB1	RML-01 and 02	417	0.05	27.4	0.01	13.55	3.02	0.14	4.11	0.01	16.3	6.84	0.1	19.85
2017RL GRAB2	RML-05	414	0.1	24	0.02	15.85	2.75	0.14	3.74	0.01	21.2	6.15	0.14	16.7
2017RL GRAB3	No thin section made	696	0.05	40.9	0.01	10.5	2.96	0.06	4.42	<0.01	6.6	4.97	0.08	19.6
2017RL GRAB4	RML-04	461	0.03	37.1	0.01	12.85	3.8	0.11	3.39	0.01	9.23	4.86	0.05	20.2

APPENDIX E: MONAZITE LOCATIONS

Sample	Location	Relationship
CLL-01 (n=1)	3500 copper orebody	In silica dolomite as part of what appears as a mineral remobilisation vein
CLL-02 (n=2)	3500 copper orebody	Isolated grain in silica dolomite; at contact between cpy and silica dolomite
RML-01 (n=1)	28B N67 NEXC, which links the 3000 and 3500 orebodies	Isolated grain within cpy
RML-04 (n=1)	28B N67 NEXC	Isolated grain in galena
RML-05 (n=1)	28B N67 NEXC	Isolated grain in silica dolomite
6055 (n=2)	500 copper orebody, lode material	Isolated grains within cpy
6080 (n=4)	V30 vertical. 11/L 423	In silica dolomite as part of what appears as a mineral remobilisation vein
6084 (n=6)	V30 East decline. 11/L 80	Isolated grains within cpy
6086 (n=3)	V30 East Decline. 11/L 1361	Within cpy, at contact between cpy and silica dolomite with pyrite/cobaltite atoll adjacent
6111 (n=1)	T14 East Decline No-2, 11/L. 518	Isolated grain in silica dolomite
6263 (n=4)	650 copper orebody – Z.74 W. Incline 12 level	Within cpy, at contact between cpy and silica dolomite with pyrite/cobaltite atoll adjacent; within silica dolomite